https://doi.org/10.5194/essd-2024-84
Preprint. Discussion started: 3 April 2024

Open Access Earth System Science Data Discussions

WetCH$_4$: A Machine Learning-based Upscaling of Methane Fluxes of Northern Wetlands during 2016-2022

Qing Ying[1*], Benjamin Poulter[2], Jennifer D. Watts[3], Kyle A. Arndt[3], Anna-Maria Virkkala[3], Lori Bruhwiler[4], Youmi Oh[4,5], Brendan M. Rogers[3], Susan M. Natali[3], Hilary Sullivan[3], Luke D. Schiferl[6], Clayton Elder[7], Olli Peltola[8], Annett Bartsch[9], Amanda Armstrong[2], Ankur R. Desai[10], Eugénie Euskirchen[11], Mathias Göckede[12], Bernhard Lehner[13], Mats B. Nilsson[14], Matthias Peichl[14], Oliver Sonnentag[15], Eeva-Stiina Tuittila[16], Torsten Sachs[17], Aram Kalhori[17], Masahito Ueyama[18], Zhen Zhang[1,19*]

[1]Earth System Science Interdisciplinary Center, University of Maryland, College Park, MD 20740, USA
[2]Biospheric Sciences Laboratory, NASA Goddard Space Flight Center, Greenbelt, MD 20771, USA
[3]Woodwell Climate Research Center, Falmouth, MA 02540, USA
[4]NOAA ESRL, 325 Broadway, Boulder, Colorado, USA
[5]Cooperative Institute for Research in Environmental Sciences (CIRES), University of Colorado, Boulder, CO 80305, USA
[6]Lamont-Doherty Earth Observatory, Columbia University, Palisades, NY, USA
[7]Jet Propulsion Laboratory, Pasadena, CA, USA
[8]Natural Resources Institute Finland (Luke), Latokartanonkaari 9, Helsinki, 00790, Finland
[9]b.geos, Korneuburg, Austria
[10]Department of Atmospheric and Oceanic Sciences, University of Wisconsin, Madison, WI 53706, USA
[11]Institute of Arctic Biology, University of Alaska, Fairbanks, AK 99775, USA
[12]Max Planck Institute for Biogeochemistry, Jena, Germany
[13]Department of Geography, McGill University, Montreal, QC H3A 0B9, Canada
[14]Department of Forest Ecology and Management, Swedish University of Agricultural Sciences, Umeå, Sweden
[15]Département de géographie, Université de Montréal, Montréal, QC, Canada
[16]University of Eastern Finland, School of Forest Sciences, Joensuu, Finland
[17]GFZ German Research Centre for Geosciences, Potsdam, Germany
[18]Graduate School of Agriculture, Osaka Metropolitan University, Japan
[19]National Tibetan Plateau Data Center (TPDC), State Key Laboratory of Tibetan Plateau Earth System, Environment and Resource (TPESER), Institute of Tibetan Plateau Research, Chinese Academy of Sciences, Beijing, 100101, China

Correspondence to: Qing Ying (qying@umd.edu)

https://doi.org/10.5194/essd-2024-84
Preprint. Discussion started: 3 April 2024

Earth System Science Data Discussions
Open Access

Abstract

Wetlands are the largest natural source of methane (CH_4) emissions globally. Northern wetlands (>45° N), accounting for 42% of global wetland area, are increasingly vulnerable to carbon loss, especially as CH_4 emissions may accelerate under intensified high-latitude warming. However, the magnitude and spatial patterns of high-latitude CH_4 emissions remain relatively uncertain. Here we present estimates of daily CH_4 fluxes obtained using a new machine learning-based wetland CH_4 upscaling framework (WetCH_4) that applies the most complete database of eddy covariance (EC) observations available to date, and satellite remote sensing informed observations of environmental conditions at 10-km resolution. The most important predictor variables included near-surface soil temperatures (top 40 cm), vegetation reflectance, and soil moisture. Our results, modeled from 138 site-years across 26 sites, had relatively strong predictive skill with a mean R^2 of 0.46 and 0.62 and a mean absolute error (MAE) of 23 nmol m^{-2} s^{-1} and 21 nmol m^{-2} s^{-1} for daily and monthly fluxes, respectively. Based on the model results, we estimated an annual average of 20.8 ±2.1 Tg CH_4 yr^{-1} for the northern wetland region (2016-2022) and total budgets ranged from 13.7 - 44.1 Tg CH_4 yr^{-1}, depending on wetland map extents. Although 86% of the estimated CH_4 budget occurred during the May-October period, a considerable amount (1.4 ±0.2 Tg CH_4) occurred during winter. Regionally, the West Siberian wetlands accounted for a majority (51%) of the interannual variation in domain CH_4 emissions. Significant issues with data coverage remain, with only 23% of the sites observing year-round and most of the data from 11 wetland sites in Alaska and 10 bog/fen sites in Canada and Fennoscandia, and in general, Western Siberian Lowlands are underrepresented by EC CH_4 sites. Our results provide high spatiotemporal information on the wetland emissions in the high-latitude carbon cycle and possible responses to climate change. Continued, all-season tower observations and improved soil moisture products are needed for future improvement of CH_4 upscaling. The dataset can be found at https://doi.org/10.5281/zenodo.10802154 (Ying et al., 2024).

Keywords
Arctic-boreal wetland; methane (CH_4) flux; eddy covariance; remote sensing; machine learning; data-driven upscaling

1. Introduction

Methane (CH_4) is the second most important greenhouse gas after carbon dioxide (CO_2) and has contributed to around 1/3 of anthropogenic warming (IPCC AR6, 2023). Wetlands are the largest natural source of CH_4 emissions. Northern freshwater wetlands (>45° N) account for roughly 40% of global wetland area (ranging 1.3 - 8.7 million km^2; Z. Zhang et al., 2021) yet the amount of CH_4 emissions from this region is highly uncertain – currently estimated to be 22 – 49.5 Tg CH_4 yr^{-1} (Aydin et al., 2011; Baray et al., 2021; Heimann, 2011; Kirschke et al., 2013; Peltola et al., 2019; Saunois et al., 2020; Treat et al., 2018; Watts et al., 2023). The uncertainties in the estimates of wetland CH_4 emissions are primarily attributed to challenges in

https://doi.org/10.5194/essd-2024-84
Preprint. Discussion started: 3 April 2024

mapping vegetated wetlands versus open water leading to double counting, seasonal wetland dynamics and uncertainties in estimates on flux rates.
Characterized by nutrient, moisture and hydrodynamic conditions, northern freshwater wetlands are classified to wet tundra in treeless permafrost areas, peat-forming bogs and fens in boreal biomes, with some exceptions (Olefeldt et al., 2021; Kuhn et al., 2021). Olefeldt et al. (2021) estimated wetland type areas in the boreal-Arctic region (0.31-0.53 million km^2 in wet tundra, 1.38-2.41 million km^2 in bogs, and 0.76-1.14 million km^2 in fens). Distinct CH_4 fluxes have been observed from wet tundra (Fig. S4, mean ± standard deviation: 13 ±14 nmol m^{-2} s^{-1}), bogs (22 ±26 nmol m^{-2} s^{-1}) and fens (56 ±88 nmol m^{-2} s^{-1}). The rates of CH_4 emissions may increase at a faster pace because of intensified warming in the Arctic (Masson-Delmotte et al., 2021; Rawlins et al., 2010; Rößger et al., 2022; Walsh, 2014; Z. Zhang, Poulter, et al., 2023).

Northern wetlands may account for a portion of the recent increase in global surface emissions in 2020 relative to 2019 (6.0 ± 2.3 Tg CH_4 yr^{-1}) (S. Peng et al., 2022; Z. Zhang, Poulter, et al., 2023). The responses of high latitude CH_4 emissions to a warming climate, with warming soils and associated permafrost thaw, an extended soil active-layer depth and duration, and projected increases in precipitation, could enforce the positive carbon-climate feedback (McGuire et al., 2009; Natali et al., 2019). However, detailed understanding of the spatio-temporal variability of high latitude wetland CH_4 emission rates remains limited.

Field observations of gas fluxes typically measure CH_4 exchange between the land and atmosphere at sub-meter to ecosystem (100s of m to km) scales. Eddy covariance (EC) provides near-continuous measurements over ecosystem-scale footprints (5 – 100 x 10^3 m^2), the size of which matches fine to medium resolution satellite remote sensing. Typical EC measurement system records include carbon, water and energy fluxes along with environmental conditions half hourly. Long-term EC datasets can support the analysis of daily, monthly, seasonal, or interannual patterns and drivers of carbon emissions (Baldocchi, 2003). Fluxnet-CH_4 represents a first compilation of global CH_4 fluxes measured by EC towers (Delwiche et al., 2021; Knox et al., 2019), yet more EC data exists outside the network. Chambers can also measure CH_4 fluxes, though at sub-meter resolution, small spatial coverage area (Kuhn et al., 2021; Bansal et al., 2023). To avoid footprint disagreement between EC and chamber measurement techniques, we focused on EC-based CH_4 upscaling in this study.

Data-driven upscaling with empirical models, including machine learning (ML) approaches, to compute CH_4 fluxes provide independent estimates (Bodesheim et al., 2018; Jung et al., 2011) complementing process-based models and atmospheric inversions (Bergamaschi et al., 2013; Spahni et al., 2011). These approaches have been used to estimate fluxes from various ecosystems such as northern wetlands (Peltola et al., 2019; Yuan et al., 2024), Finnish tundra (Virkkala et al., 2023), global reservoirs (Johnson et al., 2021), and global aquatic ecosystems (Rosentreter et al., 2021).

Two general classes of methods have been developed for data-driven upscaling. One uses a look-up table approach and applies emission rates or emission factors via data synthesis to the corresponding land surface areas, or activity data, over the study region. Emission rates from

https://doi.org/10.5194/essd-2024-84
Preprint. Discussion started: 3 April 2024

field observations are associated with environmental drivers that have been spatially characterized and are then applied to the land covers with the same environmental drivers. For example, Rosentreter et al. (2021) collected 2,601 CH_4 flux records measured using various methods through a literature review and characterized emission rates over 15 aquatic ecosystem types to upscale global aquatic CH_4 emissions. The study provided estimates of total and per ecosystem emissions but did not produce a spatial distribution and were unable to generate temporal changes. A similar method was applied to the Boreal-Arctic Wetland and Lake CH_4 Dataset (BAWLD-CH_4), where statistical CH_4 flux rates by wetland types were analyzed for emission estimation (Kuhn et al., 2021). This method favors homogeneous ecosystems and static environments, and the results may be biased for large-scale studies where spatial heterogeneity is prevalent.

Another approach uses ML methods to upscale fluxes (Bodesheim et al., 2018; Tramontana et al., 2016; Yuan et al., 2024). ML models are developed with large training datasets. Generally, ML models can learn from high-dimensional data by optimizing many statistical parameters and identifying variables that are closely associated with spatio-temporally varied CH_4 emissions. The efficient computation cost makes it easier to apply the models over large regions at higher spatial resolutions. Among ML methods, decision-tree-based algorithms have been widely used in upscaling for the computation efficiency and prediction performance (Beaulieu et al., 2020; Jung et al., 2020; Virkkala et al., 2021; C. Zhang et al., 2020). Specifically, Random Forests (RF) was utilized in regional to global wetland CH_4 upscaling (Davidson et al., 2017; Feron et al., 2024; McNicol et al., 2023; Peltola et al., 2019) for the robustness and prevention of overfitting to noise in the input data. For example, Peltola et al. (2019) used RF and EC measurements to upscale monthly CH_4 fluxes from the Arctic-boreal wetlands at 0.25°- 0.5° spatial resolution in 2013-2014. Input into ML models are predictor variables that associate with spatiotemporal variability in CH_4 fluxes, or control the biogeochemical processes of CH_4 production, oxidation, and transport: for example, direct measurements of vegetation productivity, meteorological and soil variables; or indirect measurements of the biophysical environment.

There has been a growing interest in using remote sensing data to upscale CH_4 emissions from wetlands in recent years (Davidson et al., 2017; Virkkala et al., 2023; Watts et al., 2014, 2023). This approach involves using satellite products to quantify wetland characteristics and extent. For example, seasonal average surface reflectance of Landsat 8 images was used with point-based gas trap measurements to estimate CH_4 emissions in dry and wet seasons from Everglades' freshwater marshes (C. Zhang et al., 2020). Existing ML-based large-scale upscaling models used MODIS land surface temperature at night (LST) or enhanced vegetation index (EVI), vegetation canopy height and ancillary environmental variables from remote sensing products (McNicol et al., 2023; Ouyang et al., 2023; Peltola et al., 2019. Supporting Materials Text 1 and Table S1 for details). However, soil moisture and soil temperature, two controlling factors of freshwater wetland CH_4 fluxes (Knox et al., 2021; Yuan et al., 2022), were missing in previous ML-based regional to global upscaling studies. Surface reflectance contains information about the water-vegetation complex that affects the production and transport of CH_4 to the atmosphere (Alonso et al., 2020; Chen et al., 2013; Houborg et al., 2007; Murray-Hudson

https://doi.org/10.5194/essd-2024-84
Preprint. Discussion started: 3 April 2024

et al., 2015; Z. Wang et al., 2018). Satellite products that provide constraints on the spatiotemporal variability of soil moisture and vegetation, including Soil Moisture Active Passive (SMAP) microwave-sensed soil moisture and Moderate Resolution Imaging Spectroradiometer Nadir Bidirectional Reflectance Distribution Function (BRDF) – Adjusted Reflectance (MODIS NBAR) data, may help predict the highly variable CH_4 fluxes (Entekhabi et al., 2010).

The goal of this study is to develop a scalable framework to upscale daily CH_4 fluxes from EC observations to northern latitude wetlands (>45° N) using the ensembled RF ML approach with a suite of reanalysis and remote sensing products representing spatiotemporal environmental conditions. Our specific objectives are to:

1. compile an updated EC-based CH_4 flux dataset that extends the temporal and spatial coverage of the Fluxnet-CH_4 database (Delwiche et al., 2021) for the northern latitudes;
2. build ensemble RF models of CH_4 fluxes at site-level based on *in-situ* measured variables and then at grid-level on gridded reanalysis inputs and constraints from satellite remote sensing; and
3. apply grid-level models to produce a 10-km gridded daily distribution of CH_4 flux product for the Arctic-boreal wetlands using bootstrapped models and their derived uncertainties (Table S1).

2. Materials and methods

2.1 Overview

The scalable framework of upscaling CH_4 fluxes from EC observations (referred to as WetCH_4 hereafter), traces changes in model performance from site to grid level, is illustrated in Fig. 1. In situ, reanalysis, and remote-sensing products were compiled as candidate predictors for modeling (Fig. 1, purple boxes; see section 2.2 for details). We first ran a feature selection, which uses ensemble RF models to choose important predictors from an extensive list of site-level predictor variables. Gridded versions of selected site variables were taken from Modern-Era Retrospective analysis for Research and Applications (MERRA2) reanalysis to model RF at grid level. We then added remote-sensing products from MODIS NBAR, SMAP soil wetness and topographic data, to strengthen the model and provide finer delineation of environment gradients based on literature and expert knowledge. The predictive performance of grid-level models with input variables at their native spatial resolution was then evaluated. We also compared model performance with those from two additional ML algorithms: support vector machines (SVM) and artificial neural network (ANN) (Fig. 1 pink boxes). The ML algorithm with the highest mean R^2 and lowest daily mean errors in model predictive performance was selected for bootstrap modeling and upscaling the 0.098° (~10km along longitudes) gridded time series of daily CH_4 fluxes and ensemble uncertainty estimation (Fig. 1 grey boxes).

https://doi.org/10.5194/essd-2024-84
Preprint. Discussion started: 3 April 2024

Open Access Earth System Science Data Discussions

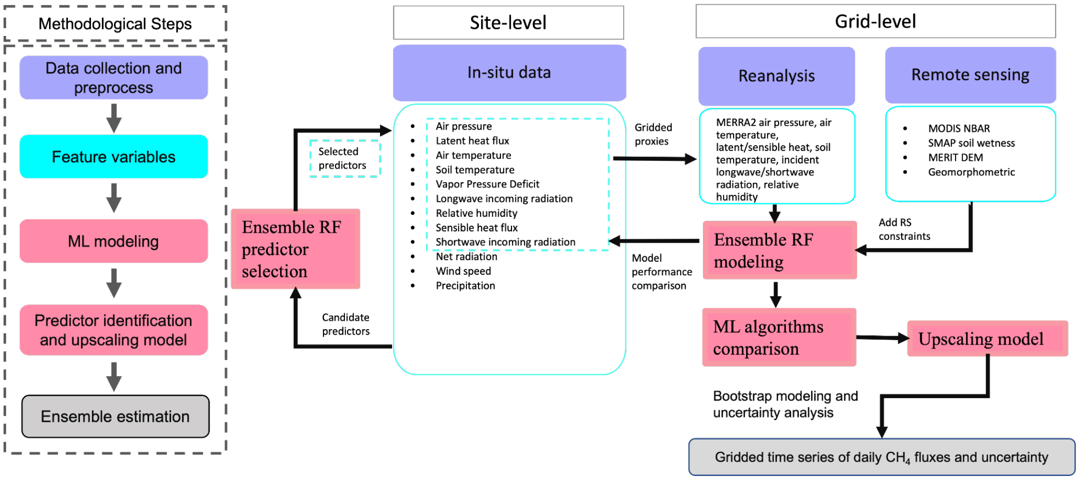

Fig. 1 Workflow and experimental design: abstract methodological steps are integrated in the dashed box on the left, while a detailed experimental design is described on the right. Colors on the right match the associated step on the left.

https://doi.org/10.5194/essd-2024-84
Preprint. Discussion started: 3 April 2024

Open Access Earth System Science Data Discussions

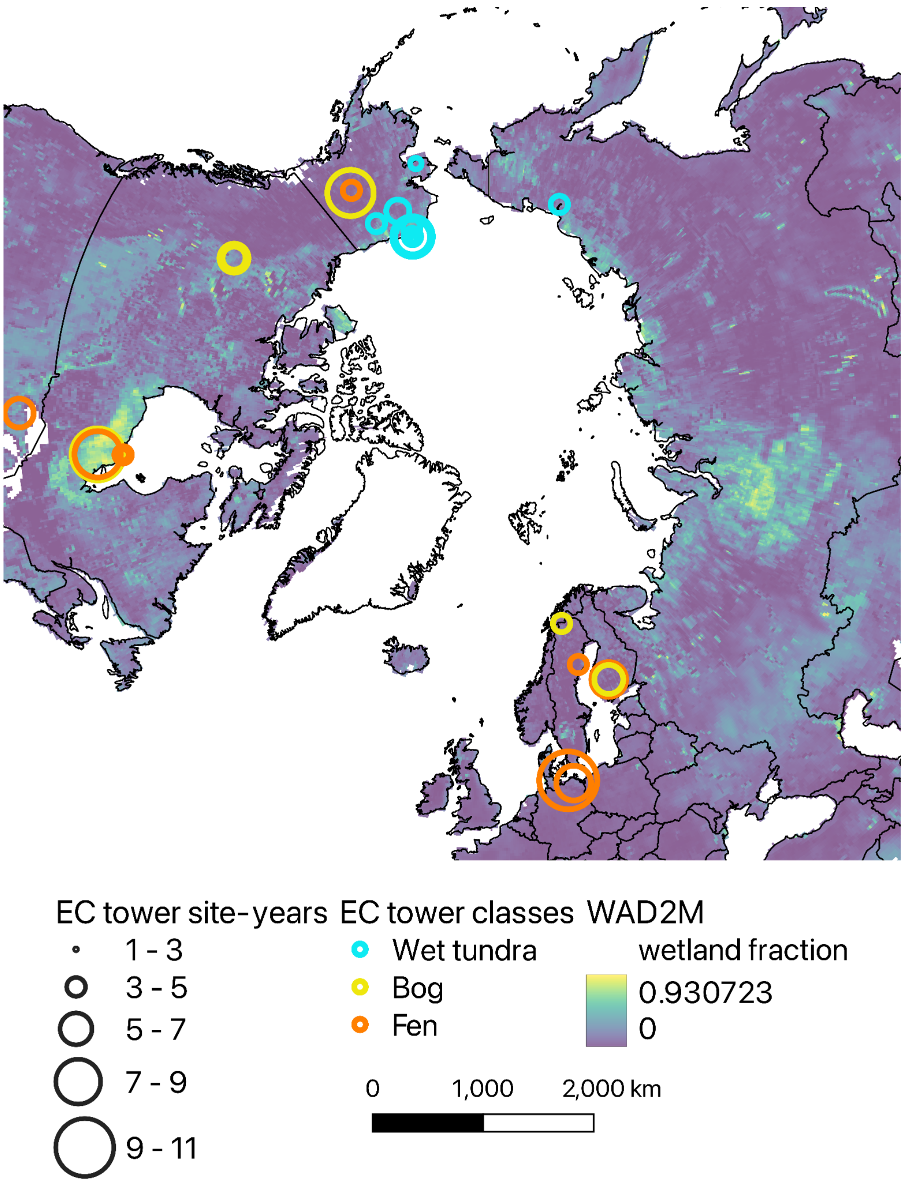

Fig. 2 Eddy covariance tower sites: distribution (>45° N), class, and data size (site-years) used in WetCH$_4$. Colored circles represent EC tower locations and land cover classes, with wetland sites in cyan (wet tundra), yellow (bog) and orange (fen). The circle sizes represent observation years(n) of available CH$_4$ fluxes at the site (e.g. 1-3 stands for 1<=n<3). The background image shows the maximum annual fractions of wetland cover in 2011-2020 from WAD2M (Z. Zhang et al., 2021).

https://doi.org/10.5194/essd-2024-84
Preprint. Discussion started: 3 April 2024

2.2 Data

2.2.1 Eddy covariance measurements

Daily and half-hourly EC data from the 26 wetland sites located in the Arctic-boreal region (>45° N) were compiled for analysis from 22 sites in FLUXNET-CH_4 (among which 8 sites with updated data to recent years, Delwiche et al., 2021; Knox et al., 2019) and 4 additional sites using information provided directly by principal investigators, consisting of 138 site-years data in total and representing the largest high latitude EC-data compilation to date (Table S2, see Supporting Materials Text 2). The sites were distributed among wetland types, including 9 fens, 7 bogs, and 10 wet tundra sites (Fig. 2). Half-hourly fluxes acquired from FLUXNET-CH_4 were already gap-filled (see Supporting Materials Text 2; Irvin et al., 2021). Additional half-hourly fluxes acquired from site PIs were not gap-filled, and we performed per site gap filling following the FLUXNET-CH_4 approach (Irvin et al., 2021; Knox et al., 2019). Gap-filled fluxes were temporally consistent and agreed with validation data (mean R^2 = 0.68 and mean RMSE = 6 nmol m^{-2} s^{-1}, *see* Supporting Materials Text 2).

The mean difference in daily mean fluxes between the gap-filled data and the original data converged to -0.2 nmol m^{-2} s^{-1} when there were more than 11 half-hourly EC tower observations in a day (Fig. S1). Therefore, daily data entries were only kept when the number of half-hourly EC tower observations per day was greater than 11. All data were retained on four sites where only daily, quality-filtered, data were provided by site PIs (Table S2). As a result, we identified 12,784 daily data entries from 26 wetland sites for upscaling models (Table S2), spanning 2015-2021 with seasonal observation distributions of 44.0% in June-July-August (JJA), 29.0% in March-April-May (MAM), 24.5% in September-October-November (SON), and 2.5% in December-January-Feburary (DJF) (Fig. S2).

Site-level candidate predictors were identified and considered to affect CH_4 fluxes at multi-day to seasonal scales during field control experiments, *in situ* flux synthesis, and process-based modeling (Bloom et al., 2010, 2017; Knox et al., 2021; Olefeldt et al., 2013, 2017). *In situ* candidate predictors that were gap-filled and available in FLUXNET-CH_4 included daily averages of air temperature, soil temperature, air pressure, vapor pressure deficit, relative humidity, latent heat flux, sensible heat flux, longwave incoming radiation, shortwave incoming radiation, net radiation, wind speed, and daily total precipitation (Fig. 1 site-level model solid blue box). We were unable to include water-table depth in our site-level model as it was not available at many sites.

2.2.2 Reanalysis data and satellite data products

Reanalysis data were used as the gridded input to replace selected predictors at site level for training the grid-level models and upscaling. These data provided long-term continuous estimates of nearly all the candidate predictors of the *in situ* measured variables (Fig. 1). MERRA2 is an atmospheric reanalysis of the modern satellite era produced by NASA's Global

https://doi.org/10.5194/essd-2024-84
Preprint. Discussion started: 3 April 2024

Modeling and Assimilation Office (Gelaro et al., 2017). We calculated daily means for air pressure, surface air temperature, latent heat flux, sensible heat flux, downward-incoming shortwave radiation, downward-incoming longwave radiation, and soil temperature at three depths (9.88 cm, 19.52 cm, 38.59 cm) (Jiao et al., 2023), and relative humidity using the hourly average of surface flux diagnostics, land surface diagnostics, and land surface forcings. The original 0.5° x 0.625° resolution data were resampled to 0.5° grids using a bilinear interpolation method in the NASA MERRA2 web service tool available on GES DISC. Daily time series of the nearest 0.5° grid to each EC location were extracted for modeling. The MERRA2 data was further bilinearly interpolated from 0.5° to 0.098° grids for the 10-km upscaling products.

To improve the predictive performance of grid-level models, we added remotely sensed biophysical variables, including SMAP soil wetness, MODIS NBAR bands, and topographic data (Fig. 1, Table 1). All remote-sensing products were extracted in daily time steps and their native spatial resolutions at EC tower sites for modeling and aggregated to 0.098° grids over the study domain for upscaling using Google Earth Engine. We filtered out data gaps in SMAP and MODIS NBAR time series extracted at the native spatial resolution during model training and validation. Gaps in MODIS NBAR were negligible when aggregated from 500-m to 0.098° grids. Gaps in winter SMAP data were filled with zero values to represent frozen soils for upscaling.

Soil moisture has been identified as one of the important, controlling factors of freshwater wetland CH_4 fluxes (Euskirchen et al., 2024; Voigt et al., 2023). Passive microwave radiometer-measured brightness temperature was merged with estimates from the GEOS Catchment Land Surface and Microwave Radiative Transfer Model in a soil moisture data assimilation system, to generate global products of surface and rootzone soil moisture (Reichle et al., 2017). In WetCH$_4$, we incorporated SMAP soil moisture to drive ML models to upscale wetland CH_4 fluxes. For soil moisture, we employed Level-4 daily soil wetness products (SPL4SMGP.007) from the SMAP mission as proxies for water-table depth in the grid-level model (Reichle et al., 2017). Surface, rootzone, and soil profile wetness are dimensionless variables that indicate relative saturation for top layer soil (0-5 cm), root zone soil (0-100 cm), and total profile soil (0 cm to model bedrock depth), respectively. These three variables are originally 3-hourly data at 9-km resolution and were converted to daily means.

Vegetation abundance and composition are influencing factors that were missing in the site-level model. Vegetation indices did not emerge as important for the predictive performance of the upscaling model in Peltola et al. (2019), probably due to their productivity measure of vegetation cover rather than vegetation types. Emergent aerenchymatous vegetation was another important component in the plant-mediated pathway of CH_4 transport yet was less represented in existing upscaling models. Land surface reflectance was utilized to map key information to emergent vegetation, vegetation composition, and inundation dynamics (Alonso et al., 2020; Murray-Hudson et al., 2015). Surface reflectance contains information about the water-vegetation complex that affects the production and transport of CH_4 to the atmosphere (Choe et al., 2021). Thus, we included MODIS NBAR (MCD43A4v061) products as predictor variables to represent the vegetation layer in the grid-level model in order to enhance our model predictive performance in vegetated wetlands. The 7 NBAR bands (including red/green/blue, 2

https://doi.org/10.5194/essd-2024-84
Preprint. Discussion started: 3 April 2024

near infrared, and 2 shortwave infrared) are developed daily at 500-m spatial resolution, using 16 days of Terra and Aqua data to remove view angle effects, and it is temporally weighted to the ninth day as the best local solar noon reflectance (Schaaf et al., 2002; Z. Wang et al., 2018).

Static topographic variables were added as additional attributes in the grid-level model. Elevation information was extracted from a multiple-error-removed improved-terrain digital elevation model (MERIT-DEM) at 90-m resolution, which significantly improves elevation estimates in flat terrain over previous DEM products (Yamazaki et al., 2017). We used topographical slope and indices that represent the water flow from MERIT-DEM based Geomorpho90m (Amatulli et al., 2020). Two topographic indices were applied: the compound topographic index (cti) is considered a proxy of the long-term soil moisture availability, and the stream power index (spi, https://gee-community-catalog.org/projects/geomorpho90/) reflects the erosive power of the flow and the tendency of gravitational forces to move water downstream. Although the DEM was significantly linearly correlated with air pressure, we still included DEM to provide fine spatial resolution gradients for coarse resolution meteorological variables from MERRA2.

Table 1. Description of input variables for grid-level upscaling model

Variable type	Name	Description	Unit	Data source	Native Spatial resolution	Native Temporal resolution
Reanalysis	tas	surface air temperature	°C	MERRA2	0.625°×0.5°	1 hourly
Reanalysis	pa	surface air pressure	Kpa	MERRA2	0.625°×0.5°	1 hourly
Reanalysis	le	latent heat	W m^{-2}	MERRA2	0.625°×0.5°	1 hourly
Reanalysis	h	sensible heat	W m^{-2}	MERRA2	0.625°×0.5°	1 hourly
Reanalysis	rsdl	downward-incoming longwave radiation	W m^{-2}	MERRA2	0.625°×0.5°	1 hourly
Reanalysis	rsds	downward-incoming shortwave radiation	W m^{-2}	MERRA2	0.625°×0.5°	1 hourly
Reanalysis	spfh	surface specific humidity	unitless	MERRA2	0.625°×0.5°	1 hourly
Reanalysis	ts1	soil temperature	° C	MERRA2	0.625°×0.5°	1 hourly
Reanalysis	ts2	soil temperature	° C	MERRA2	0.625°×0.5°	1 hourly
Reanalysis	ts3	soil temperature	° C	MERRA2	0.625°×0.5°	1 hourly
Remote Sensing	sm_s_wetness	surface soil wetness	unitless	SPL4SMGP.007	9 km	3 hourly
Remote Sensing	sm_r_wetness	rootzone soil wetness	unitless	SPL4SMGP.007	9 km	3 hourly
Remote Sensing	sm_p_wetness	profile soil wetness	unitless	SPL4SMGP.007	9 km	3 hourly
Remote Sensing	nbar1	red band	unitless	MCD43A4v061	500 m	daily
Remote Sensing	nbar2	near infrared 1 band	unitless	MCD43A4v061	500 m	daily

https://doi.org/10.5194/essd-2024-84
Preprint. Discussion started: 3 April 2024

Remote Sensing	nbar3	blue	unitless	MCD43A4v061	500 m	daily
Remote Sensing	nbar4	green	unitless	MCD43A4v061	500 m	daily
Remote Sensing	nbar5	near infrared 2 band	unitless	MCD43A4v061	500 m	daily
Remote Sensing	nbar6	shortwave infrared 1 band	unitless	MCD43A4v061	500m	daily
Remote Sensing	nbar7	shortwave infrared 2 band	unitless	MCD43A4v061	500 m	daily
Remote Sensing	dem	altitude	m	MERIT-DEM	90 m	static
Remote Sensing	slope	terrain slope	radian	Geomorpho90m	90 m	static
Remote Sensing	spi	stream power index	unitless	Geomorpho90m	90 m	static
Remote Sensing	cti	compound topographic index	unitless	Geomorpho90m	90 m	static

2.3 Machine learning model

2.3.1 General model design

We used an RF regression algorithm to construct site-level and grid-level ML models (Kim et al., 2020). RF regression builds an assembly of independent trees, each of which is trained from a random subset of input data and tested against the rest of the data (Breiman, 2001). A tree grows two leaves when a random selection of subset features reduces the mean squared error (MSE) of predictions after splitting at a leaf node. Each tree is trained on a bootstrap sample of input data. Trees constructed in this way are less correlated in the ensemble. The generalization error converges as the forest grows to a limit to avoid overfitting. Compared to other ML algorithms, RF has shown to have better accuracy and lower uncertainty (Irvin et al., 2021; Kim et al., 2020). This approach has been previously applied to upscaling CH_4 fluxes in wetlands and rice paddy (Davidson et al., 2017; Feron et al., 2024; McNicol et al., 2023; Ouyang et al., 2023; Peltola et al., 2019).

A grid-search hyperparameter tuning for daily models was performed before predictor selection. We carried out analyses in Python version 3.6 with the ensemble RF regressor in package ‘scikit-learn’ (Pedregosa et al., 2011). With all the predictors and data, hyper-parameters were set after tuning for optimized model performance, including the number of trees (n_estimators=100), number of variables to consider when looking for the best split (max_features=”sqrt”, meaning the square root of the total number of feature variables), the maximum depth of the tree (max_depth=10), the minimum number of samples required to split a node (min_sample_split=10), and the minimum number of samples at a leaf node (min_samples_leaf=4).

For predictor selection and comparisons between the site-level model using *in-situ* variables and the grid-level model using gridded versions of *in-situ* variables, we built the model across all

https://doi.org/10.5194/essd-2024-84
Preprint. Discussion started: 3 April 2024

sites and adopted 5-fold cross-validation and 'out-of-bag' scores from ensemble trees to evaluate model performance, because, at this stage, we aimed to find physically reasonable variables from *in-situ* measurements and to compare how the differences in scales and measuring methods between *in-situ* predictors and gridded proxies affect model learned temporal variability in CH_4 fluxes. A subset of data was bagged to train each tree in the RF model, with the rest out-of-bag data used as independent validation data to evaluate the prediction accuracy of each tree, resulting in the average out-of-bag scores of all the trees in the model. Cross-validation was applied to daily predictions to select variables that can best predict the daily variability of CH_4 fluxes within sites. The changes in model performance after predictor selection and after switching from site-level variables (in-situ measurements) to grid-level proxies (reanalysis data) were assessed, which helped quantify differences in model performance when modeling on *in-situ* measured predictor variables versus modeling on substitute variables at grid level.

A summary of input variables for grid-level modeling is provided in Table 1. To evaluate the impacts of adding constraint variables from remote sensing products on model performance, we designed four different model settings by changing predictor variables, including (1) only variables from MERRA2, (2) only variables from SMAP soil wetness, (3) only variables from MODIS NBAR, and (4) all predictor variables. Model predictive performance evaluates the accuracy of a model to predict at a new site without any prior knowledge. For the spatial predictive performance evaluation of grid-level ML models, we used a nested leave-one-site-out cross-validation scheme (LOOCV, hereafter). Such a scheme selects one site to use as independent validation data to evaluate models trained and tested with data from the remaining sites, repeating the process for all sites. Without any prior knowledge of the validation site added to a model, the LOOCV scheme can assess the predictive ability of the model in a new place as well as evaluate the uniqueness of a site in the dataset. Similar forms of spatial LOOCV have been used to evaluate upscaling models for global or regional CO_2 and CH_4 (McNicol et al., 2023; Peltola et al., 2019; Virkkala et al., 2021). The validation of the upscaling model was not only performed with respect to daily predictions, but also on monthly means. The predictive performance of the upscaling model on monthly variability of CH_4 fluxes and spatial variability across sites is important for studies that vary in temporal and spatial scales.

Model predictive performance was assessed using three evaluation metrics: mean absolute error (MAE), root mean squared error (RMSE), and R^2 score. Daily modeled CH_4 fluxes were compared to EC observations at each validation site. The three-evaluation metrics were calculated at daily and monthly scales for each site separately to examine the model performance by wetland types and for all sites pooled together to evaluate the overall performance and compare with existing studies. Squared error metrics are more sensitive to outliers and highly skewed data, which is often the case with CH_4 fluxes. Therefore, we selected both MAE and RMSE to quantify the errors. The mean error (ME) between model predictions and validation data was calculated, representing systematic bias in predicted fluxes. The standard deviation of model residuals was also included to measure the spread of the residuals. This matches RMSE when ME equals zero.

https://doi.org/10.5194/essd-2024-84
Preprint. Discussion started: 3 April 2024

Two additional ML algorithms were compared with RF: SVM and ANN. SVM is efficient with sparse data where the dimension of the input space is greater than the number of training samples (Kuter, 2021). While the training process of ANN is expensive and time-consuming, it can develop deep networks with growing training data (Saikia et al., 2020). We used support vector regression to model CH_4 fluxes with the same predictor variables and dataset as used in ensemble RF regressions. Multilayer perceptron regressor is an implementation of an ANN model that adjusts the weights of neurons using backpropagation to improve prediction accuracy. It uses the square error as the loss function and a stochastic gradient-based optimizer ‘adam’ for weight optimization. We used two hidden layers in the ANN model, each with 50 neurons. Data from all variables were normalized to achieve the best model performance of SVM and ANN.

2.3.2 CH_4 fluxes upscaling

We trained 500 ensemble RF models with predictors of grid-level models from the general model design and with data from all sites for upscaling daily CH_4 fluxes. Each RF model was trained with the same optimized hyper-parameters and different bootstrap samples. Ensemble models were then applied to 0.098° gridded predictors to produce the upscaling CH_4 flux intensities from the means of the 500 predictions and the prediction uncertainty from the standard deviations. Given that the CH_4 fluxes were modeled with data from the wetland EC sites, a wetland extent map was also needed to constrain the areas when scaling grid emissions (see section 2.4). Final CH_4 emission and uncertainty maps associated with wetland extents were the results of multiplying the predicted means and standard deviations of flux intensities with wetland areas. All wetland maps were resampled to 0.098° x 0.098° resolution for producing the emission products.

2.4 Wetland extent maps and benchmark estimates of wetland CH_4 emissions

Wetland extent maps were applied to scale the modeled CH_4 flux intensities to the region. The Wetland Area and Dynamics for CH_4 Modeling (WAD2Mv2), representing spatiotemporal patterns of inundated vegetated wetlands at 0.25° resolution, was selected as the reference for dynamic wetland areas in this study (Z. Zhang et al., 2021). Active and passive microwave detected inundation combined with static wetlands were used to delineate the monthly dynamics of wetland inundation between 2000 and 2020. Open water bodies such as lakes, rivers, reservoirs, coastal wetlands, and rice paddies were excluded. We used monthly mean WAD2M fractions between 2010 and 2020 to represent seasonal wetland dynamics. Emission estimations are subject to differences in the wetland extent between maps (Saunois et al., 2020). We used monthly means of the Global Inundation Extent from Multi-Satellites (GIEMS2) product (Prigent et al., 2020) to represent temporal patterns of the restricted wetland extents at 0.25° resolution. The coarse resolution maps were resampled to 0.098° x 0.098° grids using the nearest neighbor method. The static Global Lakes and Wetlands Database version 1 (GLWDv1) Level 3 1-km resolution map excluding classes of lakes, rivers, and reservoirs (Lehner & Döll, 2004) was included to quantify the upper limit of wetland cover, representing the maximum

https://doi.org/10.5194/essd-2024-84
Preprint. Discussion started: 3 April 2024

potential emission surface. For all explicit GLWDv1 wetland classes, we assumed a 100% wetland coverage in the original pixels, except for 'intermittent wetland/lake' for which we assumed a 50% coverage; for GLWDv1 classes represented as extent ranges, we used the average value of the range (i.e., 75% for 50-100% wetland, 37% for 25-50% wetland, and 12% for 0-25% wetland). To support domain emission comparisons, wetland cover was also extracted from the updated GLWD version 2 dataset (GLWDv2) which provides the spatial extent of 33 waterbody and wetland classes at 500-m spatial resolution. All freshwater wetland classes that occur in our study area (classes 8-25) from GLWDv2 were included (i.e., excluding rivers, lakes, reservoirs and other permanent open water bodies, as well as coastal saline/brackish wetlands). The original wetland areas per GLWDv2 pixel were summed across all included classes to derive a total wetland area per pixel. Furthermore, a regional freshwater wetland distribution dataset was calculated from a permafrost region specific land cover map (CALU - circum-Arctic landcover units) which classified 23 land covers including 3 wetland classes and 10 moist to wet tundra classes at 10-m resolution and aggregated to 1km with the majority class (Bartsch et al., 2023b, 2023a). This regional wetland map was applied for CH_4 emission estimation in the North Slope region in Alaska, where seasonal soil saturation was thought to be underestimated by WAD2Mv2 and GLWDv1. Wetland areas from the finer resolution maps were aggregated to 0.098° x 0.098° grids for emission calculations.

We compared WetCH_4 emissions with benchmark domain or regional estimates from bottom-up process models, top-down atmospheric observation-based inversions, and existing upscaling studies. We acquired data for the study domain from the ensemble mean of bottom-up process-based models from the Global Carbon Project (GCP) (Z. Zhang, Bansal, et al., 2023) and the extended ensemble of wetland CH_4 estimates that were priors for the top-down GEOS-Chem atmospheric chemical and transport model (WetCHARTs) (Bloom et al., 2017; Friedlingstein et al., 2022). We also included the atmospheric inversions of northern high latitudes from an assimilation CarbonTracker-CH_4 system (Bruhwiler et al., 2014; update at https://gml.noaa.gov/ccgg/carbontracker-ch4/carbontracker-ch4-2023/). We compared WetCH_4 with existing upscaled products of monthly CH_4 wetland fluxes based on Peltola et al. (2019) and McNicol et al. (2023) for the study domain. For regional wetland hotspots, CH_4 flux estimates were obtained from Carbon in Arctic Reservoirs Vulnerability Experiment (CARVE), which measured total atmospheric columns of CO_2, CH_4, and carbon monoxide over North Alaska in spring, summer, and early fall between 2012 and 2014 (R. Y.-W. Chang et al., 2014; Miller et al., 2016). We validated our seasonal emissions in the North Slope region with estimates from CARVE (Zona et al., 2016).

https://doi.org/10.5194/essd-2024-84
Preprint. Discussion started: 3 April 2024

3. Results

3.1 Model validation

3.1.1 Site-level modeling

Site-level modeling used all wetland sites to build a RF model and identified the 10 most important variables measured in situ that, if left out, decreased the valuation score of the model by more than 90% based on the mean decrease in impurity (Fig. S3). With bootstrap sampling and using all candidate predictors (Fig. 1) in the model, the out-of-bag RMSE of the site-level model was 30.22 nmol m^{-2} s^{-1}, and the out-of-bag R^2 between observed daily means of CH_4 fluxes and prediction was 0.73. Modeling with the 10 most important variables at site level resulted in similar model performance, with an out-of-bag RMSE of 30.43 nmol m^{-2} s^{-1} and an out-of-bag R^2 of 0.73. We then tested building separate models according to wetland types. The out-of-bag R^2 (RMSE) was 0.85 (7.2 nmol m^{-2} s^{-1}) for bog, 0.84 (27.7 nmol m^{-2} s^{-1}) for fen, and 0.57 (34.3 nmol m^{-2} s^{-1}) for wet tundra. Modeling with the selected 10 predictors resulted in an out-of-bag R^2 (RMSE) of 0.84 (7.6 nmol m^{-2} s^{-1}) for bog, 0.84 (27.9 nmol m^{-2} s^{-1}) for fen, and for 0.53 (36.3 nmol m^{-2} s^{-1}) wet tundra. Next, we tested whether the inclusion of non-wetland sites (upland and rice sites) would affect model performance. This resulted in an out-of-bag R^2 decrease to 0.56 and RMSE increase to 38.86 nmol m^{-2} s^{-1}, which suggests that a generalized ML model over all land cover classes is not practical to reliably predict CH_4 fluxes with the current set of predictors. This is most likely due to the distinctive features of CH_4 emissions between wetlands and non-wetland classes (Fig. S4).

3.1.2 Grid-level modeling and remote sensing constraints

Substituting *in-situ* measurements of selected predictor variables with gridded MERRA2 variables slightly reduced model accuracy. For the selected variables at site level, we used gridded variables from MERRA2 reanalysis data to build a baseline grid-level model for upscaling. The out-of-bag R^2 decreased by 9.6% to 0.66 and RMSE increased by 15% to 35.43 nmol m^{-2} s^{-1} compared to the site-level model. The coarse resolution MERRA2 data captures less spatial variability of the selected physical variables compared to *in situ* EC measurements.

Our results suggest that adding predictor variables from remote sensing products significantly improves model predictive performance compared to using MERRA2 alone (Fig. 3). The medians in the baseline model of R^2, MAE, RMSE under the LOOCV scheme were 0.34, 15.4 nmol m^{-2} s^{-1} and 20.1 nmol m^{-2} s^{-1}, respectively. Modeling only with NBAR or SMAP soil wetness returned a lower R^2 and higher errors than the baseline model, whereas modeling with both baseline variables and remote sensing variables (the 'all' model setting) achieved the highest median R^2 of 0.49 with the lowest median MAE (13.5 nmol m^{-2} s^{-1}) and RMSE (19.8 nmol m^{-2} s^{-1}). Including remote sensing constraints improved models' ability to predict spatial variability in

https://doi.org/10.5194/essd-2024-84
Preprint. Discussion started: 3 April 2024

wetland CH_4 fluxes. These results confirm our selection of predictor variables for the upscaling model (Table 1).

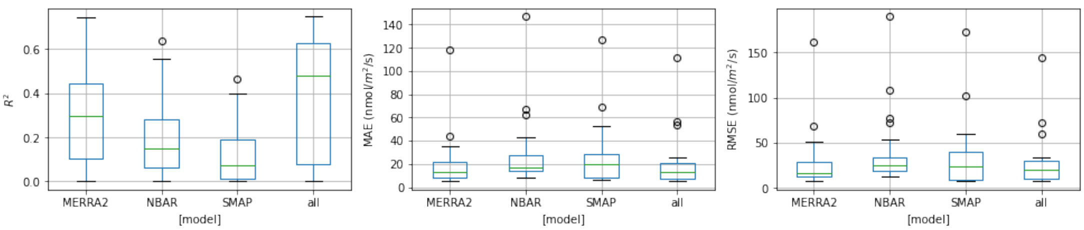

Fig. 3 Distribution of R^2, RMSE, MAE for all sites (size = 26) in a LOOCV scheme based on gridded data using four model settings: RF modeled using only MERRA2, MODIS NBAR, or SMAP soil wetness and with all variables together.

Daily mean CH_4 fluxes exhibited great variability in wetlands across space and time (mean = 35 nmol m^{-2} s^{-1}, σ = 65 nmol m^{-2} s^{-1}, Fig. S3). The model predictive performance was calculated for each site (Fig. 4a) and the average performance on the daily variability in CH_4 fluxes was best at fen sites with a mean R^2 of 0.49, followed by bog sites (0.47) and wet tundra sites (0.29). However, due to the large variability in fen daily fluxes, errors of daily predictions were highest in fen sites (mean RMSE = 39.8 nmol m^{-2} s^{-1} and mean MAE = 31.2 nmol m^{-2} s^{-1}), followed by bog sites (mean RMSE = 22.2 nmol m^{-2} s^{-1} and mean MAE =17.4 nmol m^{-2} s^{-1}), and were lowest in wet tundra sites (mean RMSE = 15.6 nmol m^{-2} s^{-1} and mean MAE =10.1 nmol m^{-2} s^{-1}). Pooling all the validation data across wetland types together, our model achieved comparable R^2 (0.46) and MAE (23.4 nmol m^{-2} s^{-1}) at the daily temporal resolution (Fig. 4b) when compared with existing ML-based upscaling studies from wetland EC CH_4 fluxes that contain similar study regions (Table 2). It is also noted that model underestimattion of fluxes (ME = -5 nmol m^{-2} s^{-1}) was driven by underestimation of fen sites (ME = -17 nmol m^{-2} s^{-1}) versus slightly overestimation of bog (ME = 8 nmol m^{-2} s^{-1}) and wet tundra (ME = 3 nmol m^{-2} s^{-1}) sites, possibly due to temperature scale discrepancies between modeling grids (0.5 deg) and EC towers (100-1000 m).

Model predictive performance on aggregated monthly means of CH_4 fluxes increased by 35% as compared to daily means (R^2 = 0.62, Fig. 4c). Performance was higher in fens (mean R^2 = 0.62) and bogs (mean R^2 = 0.70) and lower in wet tundra sites (mean R^2 = 0.37, Fig. S6). Overall errors in monthly mean predictions were: RMSE = 43.7 nmol m^{-2} s^{-1}, MAE = 21.6 nmol m^{-2} s^{-1}, and ME = -4 nmol m^{-2} s^{-1} (Table 2). Prediction residuals of daily and monthly CH_4 fluxes (Fig. S6) showed normal distributions for wet tundra sites, indicating the spread of residuals were random errors that increased with the flux magnitude. The residuals had a skewed normal distribution for bog sites indicating likely overestimation. The long-left tails in prediction residuals indicated that the intense emission fluxes from fens during summer peaks were underestimated (Fig. S6, Fig. 5b).

Site-by-site validation of daily flux predictions varied greatly between individual sites (Fig. S7). For example, US-UAF, an EC site in interior Alaska with mature black spruce cover and full

https://doi.org/10.5194/essd-2024-84
Preprint. Discussion started: 3 April 2024

understory vegetation and mosses over permafrost (Ueyama, Iwata, et al., 2023), which is the only one of the five forest bog sites in our dataset that had low CH_4 fluxes and weak seasonal cycles (less than 10 nmol m^{-2} s^{-1}), was significantly overestimated by our model (RMSE = 35 nmol m^{-2} s^{-1} and MAE = 29 nmol m^{-2} s^{-1}). Permafrost presence and ground water below soil surface may explain the low fluxes at this site (Iwata et al., 2015; Ueyama, Knox, et al., 2023). For sites with low model predictive performance, we tested if the model could learn the flux patterns at these sites if data were included in training. We found that the R^2 between daily predictions and observations improved at US-BZF (fen) and RU-CHE, US-ATQ, US-BEO (wet tundra) if data from these sites were included in training, which suggests that the unique relationships between CH_4 fluxes and predictors at these sites could not be predicted by the models trained on data from other sites and thus should be included in modeling to enhance predictive performance from spatially sparse time series data (see Supporting Materials Text 5).

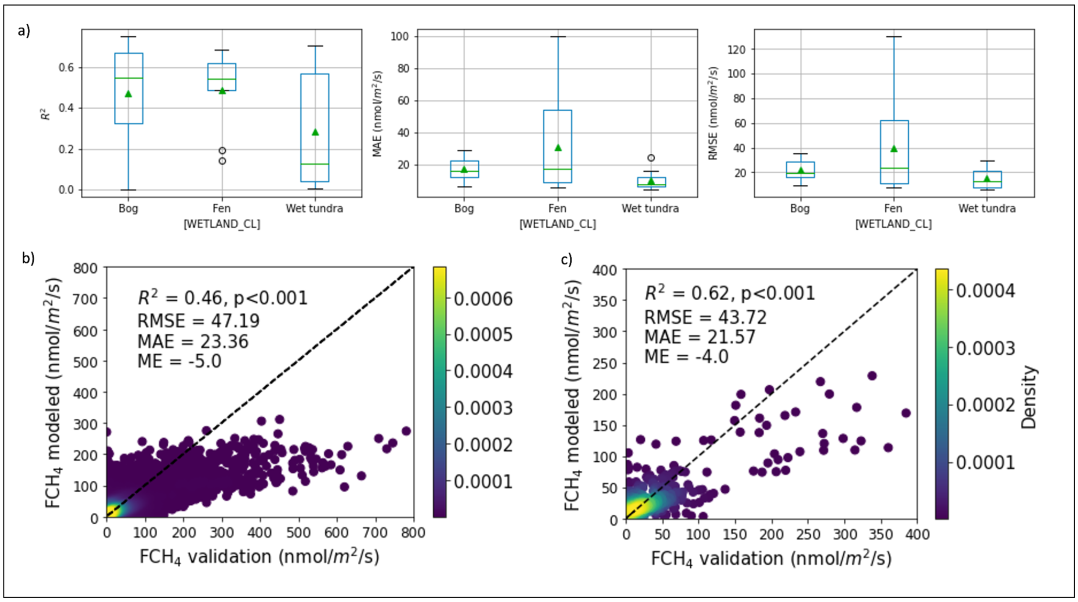

Fig. 4 Model predictive performance evaluation on RF modeled CH_4 fluxes and independent validations: (a) boxplots of R^2, MAE, and RMSE across validation sites by wetland types with mean values denoted in green triangles; (b) pooled daily means density scatter plot; (c) pooled monthly means density scatter plot.

Table 2. Comparison of model predictive performance in CH_4 fluxes with existing studies: mean R^2 and MAE of daily and monthly model predictions of all validation sites. Peltola et al. (2019) present results for the same study area.

Study	Temporal resolution	R^2	MAE (nmol CH_4 m^{-2} s^{-1})	ME (nmol CH_4 m^{-2} s^{-1})

https://doi.org/10.5194/essd-2024-84
Preprint. Discussion started: 3 April 2024

Peltola et al.	Monthly mean	0.47	22.1	0.5
McNicol et al.*	Weekly mean	0.49	36.5	-1.7
Yuan et al.	Weekly mean	0.55	38.3	/
This study	Daily mean	0.46	23.4	-5.0
	Weekly mean	0.58	23.1	-4.6
	Monthly mean	0.62	21.6	-4.0

* Numbers for the weekly evaluation metrics were for all sites from McNicol et al. as no weekly metrics was found for subregions.
/ The number was not reported in the study.

https://doi.org/10.5194/essd-2024-84
Preprint. Discussion started: 3 April 2024

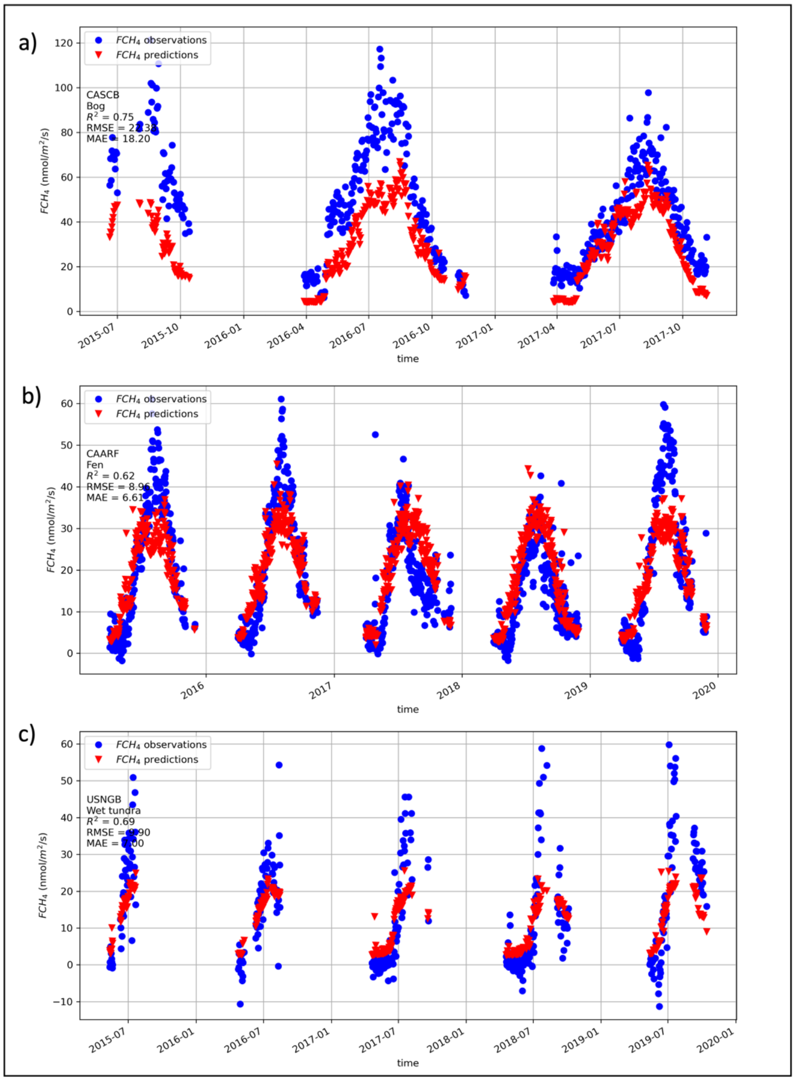

Fig. 5 Model predictive performance in seasonal cycles of daily FCH_4 at the validation sites of CA-SCB, CA-ARF, and US-NGB, representing bog, fen, and wet tundra, respectively.

The average importance of the gridded variables shows their influence on the grid-level model predictive performance (Fig. 6). Of the 24 total predictors used in the upscaling model, the first 13 variables in the mean importance rank accounted for a 74% reduction in the validation score. Importance of selected predictors under LOOCV scheme, though slightly varied between models, agreed in selecting near infrared and shortwave infrared bands (NBAR band 2, 5, and 7), SMAP rootzone and profile wetness (sm_r_wetness and sm_p_wetness), MERRA2 soil temperatures (ts1, ts2, and ts3), and DEM as the important variables in predicting daily CH_4 fluxes in northern wetlands. Nevertheless, all variables contributed to predicting variability in CH_4 fluxes, suggesting the complexity of environmental factors that would affect the rates of CH_4 production and the process of gas exchange. The mean importance of predictors in all models ranked DEM as the most important variable and sensible heat flux as the least (Fig. 6 bottom row). The Pearson correlation test between DEM and other predictor variables also show a significant correlation with surface air pressure (correlation coefficient -0.96). Elevation may therefore act as a factor in discerning sites or clusters of sites which other predictors could not differentiate.

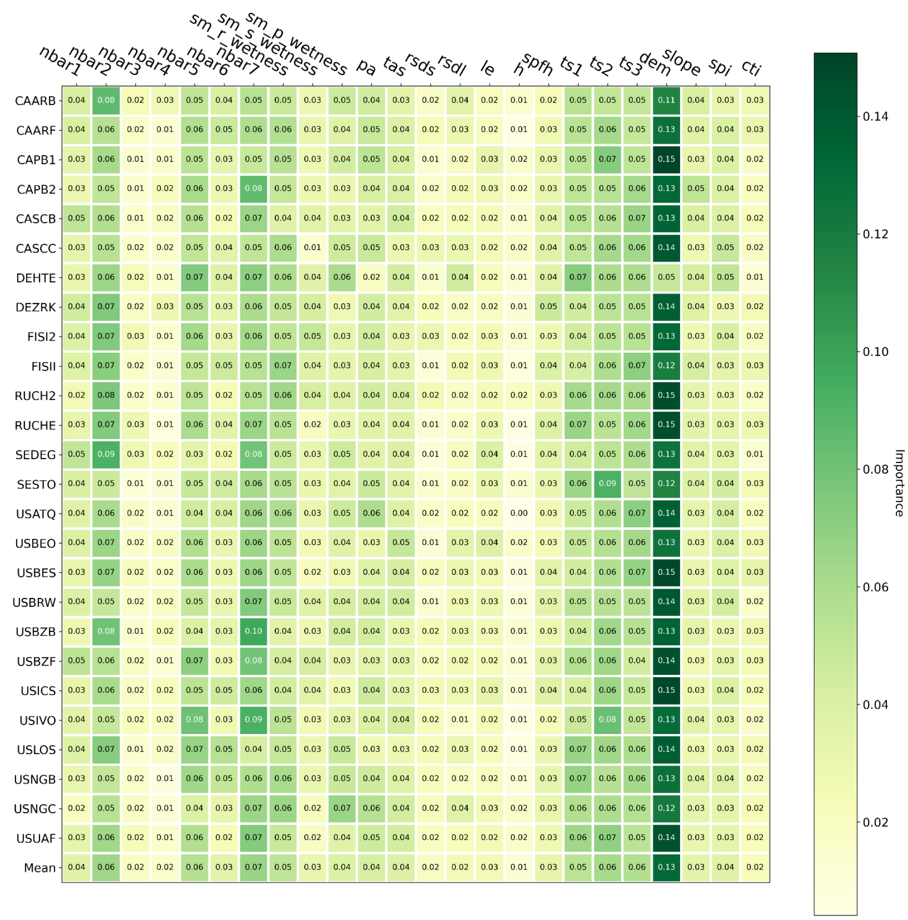

https://doi.org/10.5194/essd-2024-84
Preprint. Discussion started: 3 April 2024

Fig. 6 Mean variable importance of all models (bottom row) in the LOOCV scheme and at each site (rows labeled with validation site ID): the values in each row are the means of accumulation of the impurity decrease when a variable was taken out in the trees of a RF model, representing the importance of such variable to the model. The variable names and descriptions refer to Table 1.

3.2 Upscaled wetland CH_4 emissions

3.2.1 Wetland area weighted CH_4 emissions

Upscaled daily CH_4 fluxes were weighted by wetland fraction to estimate gridded daily CH_4 fluxes from northern wetlands based on WAD2Mv2, GIEMS2, and GLWDv1 between 2016 and 2022 (Fig. 7), and GLWDv2 for comparison. The mean annual emissions and RF model associated uncertainties are summarized with different wetland maps in Table S3. The estimate from WetCH_4 with WAD2Mv2 was 20.8 ±2.1 Tg CH_4 yr^{-1}, comparable to UpCH_4 (23.5 ±5.8 Tg CH_4 yr^{-1}). With GIEMS2, WetCH_4 estimated the minimum annual emission of 13.7 ±1.5 Tg CH_4 yr^{-1}. With GLWDv1 and GLWDv2, WetCH_4 estimated potential annual emissions of 41.0 ±4.5 Tg CH_4 yr^{-1} and 44.1 ±1.7 Tg CH_4 yr^{-1} for 2016-2022, respectively. The spatial patterns were similar to the post 2016 mean annual fluxes from GCP ensemble means of process-based models (28.6 ±21.6 Tg CH_4 yr^{-1} for 2016-2020), WetCHARTs (29.5 ±30.0 Tg CH_4 yr^{-1} for 2016-2019), and atmospheric inversions of CarbonTracker-CH_4 (40.9 Tg CH_4 yr^{-1} for 2016-2022), highlighting the intense emission areas in the Hudson Bay Lowlands and West Siberian Lowlands. The emissions from WetCH_4-GIEMS2 were lower in these two hotspots than other estimates. Differences in the distribution of CH_4 emissions between wetland products reflect the influence of wetland dynamics. Monthly wetland inundations are provided by WAD2Mv2 and GIEMS2, which set the dynamic limits for the wetland boundaries of the CH_4-emitting surface. While emissions resulting from inundation were captured, saturated or wet subsoil conditions may be missing in WAD2M and GIEMS2, resulting in low emissions in wet tundra (i.e., Alaska North Slope). To address this, we incorporated wetland fractions from the CALU high-resolution wetland map specifically produced for the permafrost region in order to estimate Alaska North Slope emissions. Wetland fractions from GLWD (both v1 and v2) represent a static maximum wetland distribution throughout time. Thus, estimates from GLWD represent the upper bounds for all northern wetlands.

https://doi.org/10.5194/essd-2024-84
Preprint. Discussion started: 3 April 2024

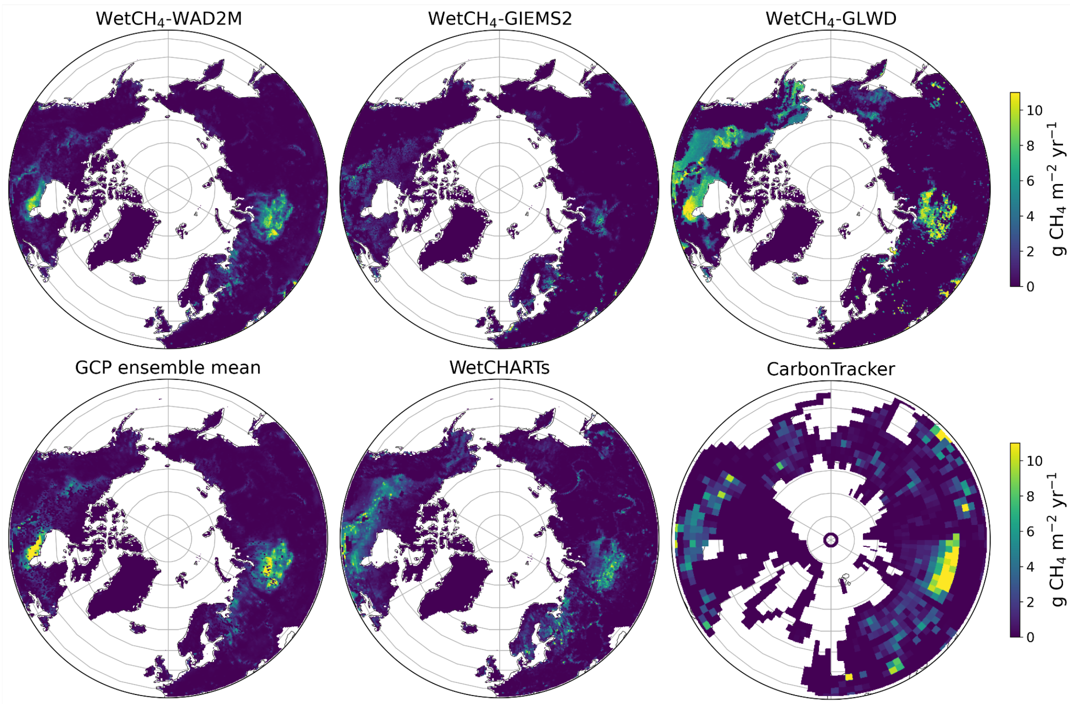

Fig. 7 Mean annual wetland CH_4 fluxes: the top row contains $WetCH_4$ upscaled fluxes between 2016 and 2022 and weighted by wetland fractions for three wetland maps WAD2Mv2, GIEMS2, and GLWDv1; the bottom row contains bottom-up GCP ensemble mean, WetCHARTs, and top-down estimates of CarbonTracker-CH_4 natural microbial emissions.

We compared spatial distributions of our upscaled fluxes ($WetCH_4$) with two alternative upscaled datasets. Using the same wetland weights, our product showed similar spatial patterns to $UpCH_4$ (McNicol et al., 2023) and the upscaled fluxes from Peltola et. al. (2019) (Fig. S9). Spatially, the maximum mean flux of 2016-2022 for $WetCH_4$ with WAD2Mv2 was 57 mg CH_4 m^{-2} day^{-1}, $UpCH_4$ produced a maximum mean flux between 2016-2018 of 88 mg CH_4 m^{-2} day^{-1}. While all three products predicted concentrated CH_4 exchange in the Hudson Bay Lowlands and West Siberian Lowlands, and low fluxes in West Canadian Arctic tundra, $WetCH_4$ predicted lower fluxes in forested wetlands of West Canada than $UpCH_4$ (Fig. S9 a,b). With GLWDv1, $WetCH_4$ predicted similar fluxes to those of Peltola et al. (2019), with the exception of a number of potent emitting grids in the West Siberian Lowlands (Fig. S9 c,d) and a maximum mean flux of 147 mg CH_4 m^{-2} day^{-1} from $WetCH_4$.

3.2.2 Seasonal cycles of wetland CH_4 emissions

Mean seasonal cycles of wetland CH_4 emissions were consistent with bottom-up estimates in the domain and top-down inversions in high latitudes (Fig. 8). The amplitudes of two ML-based estimates agreed in the domain ($WetCH_4$ and $UpCH_4$ both within WAD2Mv2 wetland areas) and

https://doi.org/10.5194/essd-2024-84
Preprint. Discussion started: 3 April 2024

were lower than the ensemble means of GCP or WetCHARTs estimates during the growing season (Fig. 8a). In the northern high latitudes (60° - 90° N), the amplitudes of this study closely agree with WetCHARTs, and both were lower than the ensemble means of GCP in the growing season (Fig. 8b). Our emissions in June-July-August were lower than the emissions attributed by the atmospheric inversion of CarbonTracker-CH_4, which does not discriminate between wetland and open water sources. We did not use comparisons with CarbonTracker-CH_4 for 45°-90° due to likely considerable contributions from aquatic systems and other non-wetland factors in the inversion estimates. Notably, uncertainties between ML-based approaches with the same wetland extents showed less variation than those between process-based models, especially during the growing season. The phase of our estimates (WetCH_4) agreed with bottom-up and top-down models, peaking in July followed by August (Fig. 8a,b), whereas UpCH_4 showed a month lag, probably due to the two- or three-week lag of predictor variables selected in UpCH_4 (McNicol et al., 2023) . Peak fluxes in July and August were commonly seen in tower measurements.

The seasonality in upscaled wetland CH_4 emissions corresponded to the intensities of fluxes and dynamics of wetland areas. We compared mean seasonal cycles of upscaled products with different dynamic or static wetland maps to constrain the impacts of wetland areas (Fig. 8c). As observed in spatial distributions (Fig. 7a,c), emissions from the potential emitting surface (WetCH_4_GLWDv1) were 73% higher than those from reference inundated wetlands (WetCH_4_WAD2Mv2) during the growing season, and doubling in winter. Within the potential emitting surface, WetCH_4 predicted higher emissions than Peltola et al. (2019) in July (21%), August (21%), December (45%), and January (71%), but 20% lower in October. Reported emissions (Zona et al., 2016) from the freezing active layer at permafrost areas in October (zero-curtain period) may not be well captured by our ML model. The differences in wetland areas between the two dynamic products (WAD2Mv2 and GIEMS2) only affected emissions in May and June in WetCH_4, but significantly affected emission magnitudes in UpCH_4. Despite the differences in wetland areas, the phases of emissions cycles of WetCH_4 were consistent with those from Peltola et al., whereas UpCH_4 again lagged a month.

We compared upscaled seasonal cycles with CH_4 fluxes estimated from regional airborne measurements taken during CARVE campaigns over the Alaska North Slope (Fig. 8d). Given that WAD2Mv2 underestimated wetland area in this region (Schiferl et al., 2022), we computed mean seasonal cycles over the land, over freshwater wetlands of CALU, and over WAD2M and Hydrolakes, representing three different scenarios. The range of our upscaled estimates aligned with regional emissions derived from CARVE measurements. Chang et al. (2014) estimated 7 ±2 mg CH_4 m^{-2} d^{-1} of mean CH_4 fluxes during the growing season in the North Slope from the column analysis of CARVE data. The mean fluxes (May to September) of WetCH_4 with CALU were estimated at 6.2 ±0.6 mg CH_4 m^{-2} d^{-1} (4.6 ±0.5 mgC CH_4 m^{-2} d^{-1}), which is within the range of various CARVE estimations (Miller et al., 2016). The landscape is in the biome of the Arctic coastal tundra and is covered by sedges, grasses, mosses, and dwarf shrubs. A large number of lakes and freshwater ponds are scattered across the area. Studies at the West Alaska lowland of Yukon–Kuskokwim Delta found aquatic fluxes that were about ten times higher than in wet tundra during September (Ludwig et al., 2023), suggesting that a major source of the

https://doi.org/10.5194/essd-2024-84
Preprint. Discussion started: 3 April 2024

airborne fluxes missing in WetCH$_4$ in the late growing season, can be attributed to open water fluxes. Emissions from wet soil may double or more if permafrost thaw expands over the land and the region becomes wetter with rising temperatures. The most remarkable increases could be in summer and winter, as indicated by the range between the green and the black lines in Fig. 8d.

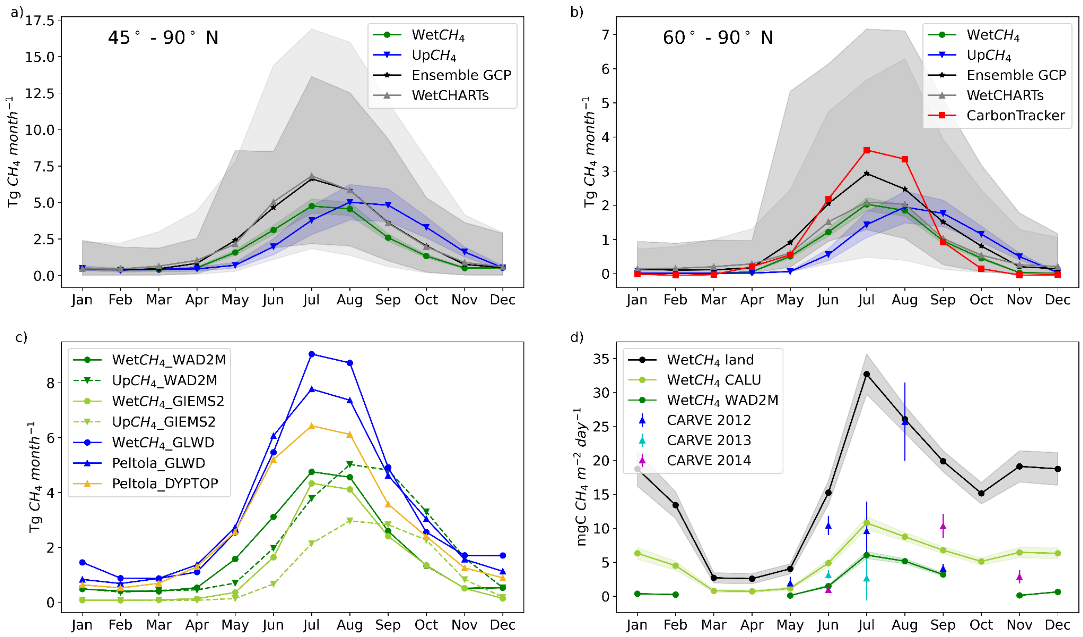

Fig. 8 Multi-year average seasonal cycles of wetland CH$_4$ emissions: (a) comparison of ML upscaled mean seasonal cycles in reference wetland areas (WAD2Mv2) with the cycles from process-based models in the northern mid-high latitudes (45° - 90° N); (b) same comparison for northern high latitudes (60° - 90° N) and addition of atmospheric CarbonTracker-CH$_4$ attributed microbial emissions (2016-2022); (c) comparison of three ML upscaled mean seasonal cycles of CH$_4$ emissions with different wetland area maps; (d) comparison of WetCH$_4$ mean seasonal cycles over the land (black line), weighted by wetland of the CALU map (olive line), or weighted by fractions of WAD2Mv2 (green line), with estimates of CH$_4$ fluxes in growing seasons from CARVE retrievals in North Slope area of Alaska (Zona et al., 2016).

3.2.3 Interannual variations in wetland CH$_4$ emissions

The mean annual emissions from ML-based estimates with WAD2M were lower than the GCP ensemble mean and WetCHARTs, despite over different years from 2016 forward (Fig. 9a). All products demonstrated similar emission patterns for the domain in the interannual trends and variations, highest in 2016 and lower for three years from 2017 to 2019 (Fig. 9). The interannual variations in WetCH$_4$ were driven by the interannual variability in the upscaled fluxes as only

https://doi.org/10.5194/essd-2024-84
Preprint. Discussion started: 3 April 2024

Open Access Earth System Science Data Discussions

multi-year mean seasonal dynamics from WAD2Mv2 were used. All products identified intensified emissions in 2016 as indicated by the variations relative to period means (Fig. 9b). Higher than period average emissions in 2020 were also modeled by WetCH$_4$ and ensemble GCP. The recent intensification from wetland emissions was discovered globally with an important contribution from northern wetlands (S. Peng et al., 2022; Yuan et al., 2024; Z. Zhang, Poulter, et al., 2023).

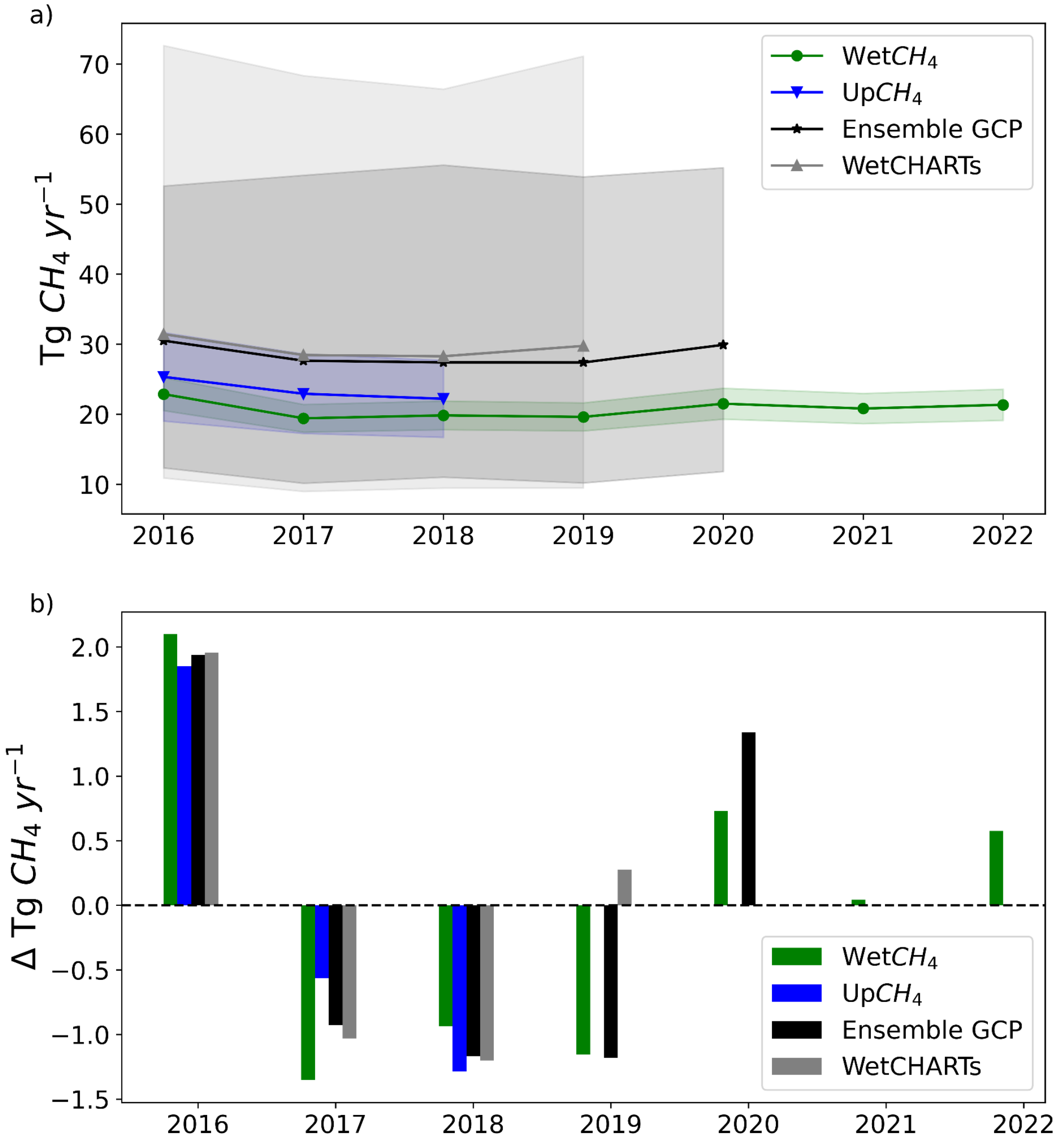

Fig. 9 Wetland CH$_4$ a) annual emissions and associated uncertainties in colored shades and b) variations relative to multi-year means in the research domain (45° - 90° N). Wetland area data

https://doi.org/10.5194/essd-2024-84
Preprint. Discussion started: 3 April 2024

applied in $WetCH_4$ and $UpCH_4$ was WAD2Mv2. Time periods of multi-year means: $WetCH_4$ (2016-2022); $UpCH_4$ (2016-2018); Ensemble GCP (2016-2020); WetCHARTs (2016-2019).

Subregional annual emissions and interannual variability (Fig. 10) of $WetCH_4$ were calculated for eight subregions in the northern high latitudes (Fig. S11): Siberian tundra, East Siberia, West Siberia, Fennoscandia, Canadian tundra, East Canada, West Canada, and Alaska. The main differences in $WetCH_4$ estimated emissions between WAD2Mv2 and GLWDv1 occurred in the East Siberia, East Canada, West Canada, and Alaska subregions. However, interannual variabilities were similar. Interannual variations from West Siberia accounted for 51% the variations in domain emissions (Fig. 10a). The positive change in East Canada canceled the negative change in West Siberia in 2021, resulting in low variability in the domain emission for that year (Fig. 9). The relative interannual variability, which was calculated as the percentage of a variation to the period mean of a subregion, was attributed to those from West Siberia, Fennoscandia, West Canada, and Alaska (Fig. 10b).

https://doi.org/10.5194/essd-2024-84
Preprint. Discussion started: 3 April 2024

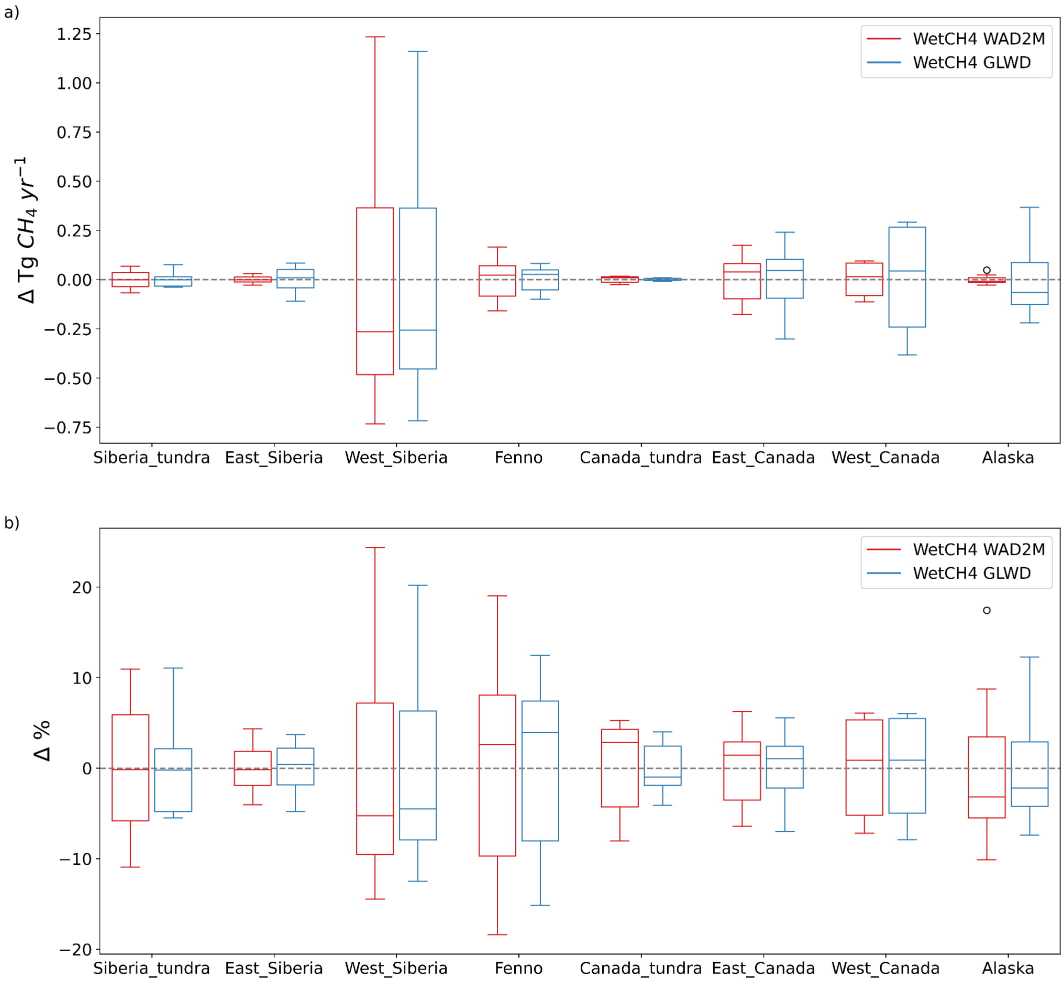

Fig. 10 Interannual variations and variability in subregions predicted by WetCH$_4$ with WAD2Mv2 and GLWDv1, respectively: (a) interannual variations with respect to period means (2016-2022); (b) relative variability as the percentage of its period mean. Delta in the y axis denotes the annual emissions minus mean annual emissions in the period 2016-2022.

4. Discussion

This study presents daily scale, data-driven 10-km wetland CH_4 fluxes for the northern terrestrial wetland region, upscaled from EC data. The upscaling framework was driven by MERRA2 meteorological variables and soil temperatures and constrained by satellite products from SMAP soil moisture and MODIS NBAR, resulting in improved prediction accuracy (R^2 = 0.62 and MAE =21 nmol m^{-2} s^{-1}) in monthly mean fluxes. Predictions of the variability (R^2) in monthly means of CH_4 fluxes increased by 30% over previous studies (Peltola et al., 2019; McNicol et al., 2023). Model agreement performed less at daily and weekly timesteps due to higher

https://doi.org/10.5194/essd-2024-84
Preprint. Discussion started: 3 April 2024

variability in CH_4 fluxes at finer temporal resolutions. In our framework, we applied a rigorous criterion on the counts of half-hourly observations to control the selection quality of daily gap-filled data, which may filter out errors introduced by the gap-filling process or lack of observations for calculating daily means. The improvement in model performance can be partly attributed to the inclusion of soil temperature, MODIS vegetation reflectance, and satellite assimilation of soil moisture in the framework that incorporates controlling factors of CH_4 fluxes recognized in field experiments and synthesis studies (Fig. 3).

4.1 Important drivers to improve RF model predictive performance

Soil temperature plays an important role in microbial growth and dormancy (Chadburn et al., 2020), and exponentially affects microbial CH_4 emission rates although the temperature sensitivity (Q_{10}) varies across space and time (Knox et al., 2021; van Hulzen et al., 1999). In northern wetlands, soil temperature is often more spatially variable relative to air temperature due to snow insulation and active layer depth (Smith et al., 2022; W. Wang et al., 2016; Yuan et al., 2022), and thus should be considered in upscaling models. Compared to air temperature or land surface temperature that were used in previous upscaling studies (Peltola et al., 2019; McNicol et al., 2023), the inclusion of MERRA2 soil temperatures in WetCH4 likely contributed to a higher model predictive performance, although the impact of scale mismatch between the native MERRA2 spatial resolution and the local footprints on the upscaled fluxes were not quantified. Independent validation studies found significant correlations in the temporal trend and seasonal cycles between MERRA2 soil temperatures and in situ observations (M. Li et al., 2020; Ma et al., 2021). However, most of the *in situ* stations were located in the U.S. and mid-latitude Eurasia. Lower correlations with overestimated monthly variability were found in the cold season in Pan-Arctic (Herrington et al., 2022), suggesting the impact of the uncertainty in MERRA2 soil temperatures on CH_4 fluxes concentrated in winters in this study.

Emergent vegetation affects the recent substrate availability and the plant-mediated transport of CH_4 (Kyzivat et al., 2022; Melack & Hess, 2023). We used the full land bands of the MODIS NBAR product rather than higher-level vegetation indices used in previous upscaling studies, as signals for vegetation and inundation dynamics are retained in remotely sensed land reflectance (Chen et al., 2013). The near-infrared and shortwave infrared bands (NBAR bands 2, 5, and 7) presented relatively high importance in our model due to their associations with vegetation productivity and water table dynamics in northern peatlands (Burdun et al., 2023). Satellite inputs provide high spatial resolution constraints on the environmental variability and help improve model spatial predictive performance (Fig. 3), indicating the requirement of high spatial resolution driving input for accurately modeling wetland CH_4 fluxes.

Surface and rootzone soil moisture also exhibits control on ecosystem anaerobic metabolism. Low soil moisture implies oxic conditions and allows methanotrophic bacteria to consume CH_4, whereas high soil moisture enables CH_4 production and suppresses consumption (Liebner et al., 2011; Olefeldt et al., 2013; Spahni et al., 2011). Soil wetness estimated at rootzone and the profile from SMAP measurements may be able to capture water-table dynamics and hence

https://doi.org/10.5194/essd-2024-84
Preprint. Discussion started: 3 April 2024

ranked as important in $WetCH_4$ model performance. Validation of the SMAP level 4 soil moisture data assimilation product has shown that it meets performance requirements (Colliander et al., 2022). However, the validation sites are mostly located in North American grassland, cropland and shrubland, requiring more *in situ* soil moisture observations in high latitude tundra and peatland. Regional validation studies suggested uncertainties of satellite derived soil moisture including SMAP at high latitudes were high (Högström et al., 2018; Wrona et al., 2017) and remained to be addressed.

Underground processes of CH_4 production and oxidation are difficult to model (Ueyama, Knox, et al., 2023), especially for seasonal cycles in the northern high latitudes. A hysteresis effect that manifests intra-seasonal variability in the dependence of CH_4 fluxes on temperature has been observed at EC sites (K.-Y. Chang et al., 2021), but it was not reproduced in $WetCH_4$. Positive hysteresis and the difference in frozen status from topsoil to deep soil during autumn freeze results in zero curtain periods that have been observed at high latitude tundra (Bao et al., 2021; Zona et al., 2016), the occurrence of which was subsequently underestimated in our model. The amount of substrate available for methanogenesis, missing in our framework, could be a controlling factor of the occurrence of this phenomenon. Higher substrate availability elevates methanogen abundance and activities during autumn freeze (Bao et al., 2021). However, spatially explicit substrate data are not available. Using proxies such as net primary production or EVI for substrate availability might be oversimplified (Larmola et al., 2010; T. Li et al., 2016; Peltola et al., 2019). In addition, the uncertainty of deep soil temperature of training inputs in late autumn may hinder the model's ability to capture patterns of high emissions during zero curtain periods observed at Alaska tundra (Fig. S10). More temporally accurate soil temperature data is needed to delineate the soil freezing progress and properly constrain predictions of CH_4 emission during the cold season (Arndt et al., 2019). The $UpCH_4$ results (McNicol et al., 2023) also suggest that simply imposing lags to temporal predictors in RF cannot capture complex intra-seasonal variability due to the complicated lag effects interacting with the water table depth (Turner et al., 2021). Without timestamps in predictors, RF treats time series fluxes independently, which may limit its predictive performance. Deep learning models designed to account for temporal progress in data, such as Long Short Term Memory (LSTM) neural networks, may improve modeling accuracy of seasonal cycles (Reichstein et al., 2019; Yuan et al., 2022).

4.2 Data limitations in current EC CH_4 observations

Data deficiency in winter and in under-represented areas limited the RF model's extrapolation ability. Data abundance and representativeness across space, time, and wetland types drives model performance and ability to extrapolate for the data-driven approach. The 26 wetland EC sites included in this study are largely located in Fennoscandia, East Canada and Alaska (Fig. 2), leaving some emission hotspots under-represented. For instance, Western Siberian Lowlands, the large wetland complex and the major contributor of interannual variations of CH_4 in the region, has limited data that is compiled from a single site (RU-VRK, not included in this study due to the observations before our study period). Cold season emissions could contribute

https://doi.org/10.5194/essd-2024-84
Preprint. Discussion started: 3 April 2024

a substantial fraction of the Arctic tundra annual CH_4 budget (Mastepanov et al., 2008; Mavrovic et al., 2024; Zona et al., 2016). But after filtering, 23% of the EC data in high latitudes (>60° N) were recorded between November and March, which could be insufficient for accurately modeling zero curtain period fluxes.

Ten bog and fen sites used for modeling contain all season daily flux records with half-hourly observations more than 11, all from Fennoscandia and Canada. Although Alaska is represented by 11 wetland sites, sufficient winter observations with good quality are still needed. West Siberian Lowlands are underrepresented by EC CH_4 sites. Missing data in MODIS NBAR due to snow cover or gaps in SMAP reduced training data by 31% and 48% in the study domain, respectively. Filling data of MODIS NBAR to account for snow cover information and gap-filling SMAP soil moisture products can make full use of available EC observations and help improve model performance in cold seasons. Many wetland sites in the study are located in areas with peatland presence, with 35% of sites in peatland-rich areas with >50% peatland cover (Hugelius et al., 2020). More tower CH_4 measurements over mineral wetlands need to be included in future upscaling studies. Wetlands with soil materials containing less than 12% organic carbon by weight are considered mineral wetlands. High-emitting marshes, though covering only 5% of the total wetland area in the boreal-Arctic domain, need to be considered when deploying new EC sites (Kuhn et al., 2021; Olefeldt et al., 2021). This study identified CH_4 emission hotspots and areas undergoing strong interannual variations, which are yet not part of the current FLUXNET network. The wall-to-wall flux maps also provide spatially continuous information for effectively further developing the CH_4 flux tower network.

4.3 Budget comparison

WetCH4 estimated annual and seasonal mean emissions that were comparable to existing data-driven products in the study domain (Table S3). With the dynamic WAD2Mv2 map, our estimation was 2.7 Tg CH_4 yr^{-1} smaller than UpCH4 due to a larger bias in WetCH4 and the mean seasonal cycles between 2010 and 2020 from WAD2M applied in our estimation. With the same static GLWDv1 map, our estimation was about 10% larger than the estimate from Peltola et al. (37.5 ±12 Tg CH_4 yr^{-1} for 2013-2014) despite the different periods. This is attributed to higher fluxes estimated by WetCH4 in DJF and JJA seasons. With two versions of the static GLWD maps, we estimated potential annual emissions between 41.0 and 44.1Tg CH_4 yr^{-1}. Compared to GLWDv1, version 2 of GLWD mapped smaller wetland fractions in the Hudson Bay Lowlands with intense CH_4 fluxes and more wetlands in the northwest of the Ural Mountains, Eastern Siberia, and the Sanjiang Plain, where CH_4 intensities were weaker, resulting in a larger estimate of the annual emission (Fig. S13). The wide range of data-driven estimates was driven by the differences in wetland maps. While WAD2M provides crucial information on wetland inundation dynamics controlling interannual and inter-seasonal changes in CH_4 emitting areas, areas with saturated soil in the Arctic tundra in summer are underestimated (Fig. 8d), requiring more accurate maps in delineating the dynamic wet tundra. Overall, accurate and dynamic wetland maps in high spatial resolution are needed to tackle the uncertainty in the wetland emission budget. Bottom-up estimates on wetland CH_4 emissions

https://doi.org/10.5194/essd-2024-84
Preprint. Discussion started: 3 April 2024

from data-driven, GCP ensemble means and WetCHARTs are smaller than the top-down CarbonTracker-CH_4 estimate on natural microbial emissions because the latter includes emissions from aquatic systems. CH_4 emissions were estimated at 4.7 Tg CH_4 yr^{-1} from rivers and streams (Rocher-Ros et al., 2023) and 9.4 Tg CH_4 yr^{-1} from lakes (Johnson et al., 2022) in the Arctic and boreal region (>50°N). The total emissions estimated from wetlands and open water are comparable to the CarbonTracker-CH_4 estimate. The amplitudes of WetCH_4 seasonal mean fluxes align with bottom up and top down estimates. Differences in the seasonal dynamics of wetland maps are the major source of upscaling uncertainty and result in various uncertainties between regional estimates. While atmospheric inversion models need bottom-up estimates as priors, data-driven upscaled CH_4 products offer alternatives to process-based estimates to assist with inversion models in regions where data-driven models perform well (Bloom et al., 2017; Melton et al., 2013).

4.4 Future directions

The future development of EC network in the northern high latitudes will provide more observations, which can enable monitoring and modeling changes in CH_4 fluxes. Deploying new sites in under-represented areas will not only benefit flux upscaling efforts but also our understanding of how ecosystem metabolism responds to the changing climate (Baldocchi, 2020; Pallandt et al., 2022; Villarreal & Vargas, 2021). With the availability of long-term predictor variable data, it is possible to expand our WetCH_4 upscaling framework for longer periods (e.g., 2000 to current), when adequate flux observations in 2000-2010 from chambers are compiled since 96% of the data were recorded after 2010 in FLUXNET-CH_4 (McNicol et al., 2023).

Several data products exist for the meteorological predictor variables. Quantifying measurement uncertainties between products of predictor variables and how the uncertainties propagate to upscaling products need to be addressed in future work. The mismatch of spatial scales between tower footprints and predictor variables may cause underestimation of abruptly high fluxes measured at tower landscapes when environmental conditions are averaged over half-degree grids (Chu et al., 2021; McNicol et al., 2023). Therefore, downscaling predictor variables for developing higher-resolution products is needed, especially for the Arctic region where thermokarst development is shaping permafrost landscapes with fragments of wetlands, thermokarst ponds, and forests (Miner et al., 2022; Osterkamp et al., 2000; Wik et al., 2016). For example, Fang et al. (2022) have downscaled global SMAP surface soil moisture to 1-km resolution, and Optical/Thermal and microwave fusion methods have been developed to downscale soil moisture (J. Peng et al., 2017). Nevertheless, downscaled products for rootzone or profile soil moisture are needed for upscaling CH_4 fluxes as are soil temperature products.

Beyond the ML-based upscaling framework, hybrid modeling of the data-driven approach and process-based models is a promising but also challenging direction of future study (Reichstein et al., 2019). One practice constrained regional data-driven fluxes with top-down estimates via auto-learned weights on per pixel fluxes in a region (Upton et al., 2023). Another practice pretrained a time-dependent ML algorithm with initialization from process-based synthetic data

https://doi.org/10.5194/essd-2024-84
Preprint. Discussion started: 3 April 2024

Open Access Earth System Science Data Discussions

and then fine-tuned the model with observations (Liu et al., 2022). Finally, leveraging physical constraints to increase the interpretability of data-driven models and computation efficiency is still an important factor to consider in all hybrid modeling.

5. Code and data availability

The daily CH_4 flux intensities in the northern wetlands at a spatial resolution of 0.098° x 0.098°and associated uncertainties, along with daily emissions weighted by WAD2M, GIEMS2, and GLWDv1, can be accessed through https://doi.org/10.5281/zenodo.10802154 (Ying et al., 2024). Source code of ML modeling and upscaling is publicly available at https://github.com/qlearwater/WetCH4.git. Half-hourly EC data is available for download at https://fluxnet.org/data/fluxnet-ch4-community-product/ (Delwiche et al., 2021).

6. Conclusions

We developed an ML framework (WetCH_4) to upscale daily wetland CH_4 fluxes of mid-high northern latitudes at 10-km spatial resolution combining EC tower measurements with satellite observations and climate reanalysis. WetCH_4 is novel in that it is the first upscaling framework to introduce SMAP soil moisture and MODIS reflectance in modeling wetland CH_4 fluxes to improve accuracy (R^2 = 0.62). The remote-sensing products provided high spatial resolution constraints associated with the abiotic controllers of CH_4 fluxes, indicating the importance of using high spatial resolution inputs in models for accurately simulating the spatiotemporally variable CH_4 emissions from heterogeneous northern wetland landscapes. The framework highlights the importance of soil temperature, vegetation, and soil moisture for modeling CH_4 fluxes in a data-driven approach. Using WetCH_4, an average annual CH_4 emissions of 20.8 ±2.1 Tg CH_4 yr^{-1} with WAD2Mv2 was estimated and ranged between 13.7 ±1.5 Tg CH_4 yr^{-1} with GIEMS2 and 44.1 ±1.7 Tg CH_4 yr^{-1} with GLWDv2 from vegetated wetlands (>45° N) for 2016-2022, approximately 13-30% of the global wetland CH_4 budget (Saunois et al., 2020). Differences in estimates of wetland CH_4 emissions due to different wetland maps applied, highlighting the need for high resolution wetland maps and accurate delineation of wet soil dynamics. Emissions were relatively lower in 2017-2019 and intensified in 2016, 2020 and 2022, with the largest interannual variations coming from West Siberia. Spatio-temporal distributions of CH_4 fluxes find emission hotspots and regions of intensified interannual variations that are not currently measured with EC. Comparing with current EC sites, we suggest a need for tower observations in wetlands of West Siberia and West Canada and diversified observations across wetland types. More site observations in soil water related variables are needed for improved understanding of flux controls in northern wetland ecosystems. Future wetland CH_4 upscaling work could benefit from improved soil moisture products and hybrid modeling.

https://doi.org/10.5194/essd-2024-84
Preprint. Discussion started: 3 April 2024

Open Access Earth System Science Data Discussions

Acknowledgements

This work was supported by funding catalyzed by the TED Audacious Project (Permafrost Pathways). We thank Sara Knox and Gavin McNicol for their helpful suggestions in the early stages of the compilation of EC CH_4 fluxes and the development of the upscaling product, respectively. Ben Poulter acknowledges support from the NASA Terrestrial Ecology Program. Annett Bartsch was supported by the European Space Agency CCI+ Permafrost and AMPAC-Net projects. Aram Kalhori was supported by the European Union’s Horizon Europe program, grant agreement no. 101056848.

References

Alonso, A., Muñoz-Carpena, R., & Kaplan, D. (2020). Coupling high-resolution field monitoring and MODIS for reconstructing wetland historical hydroperiod at a high temporal frequency. *Remote Sensing of Environment*, *247*, 111807. https://doi.org/10.1016/j.rse.2020.111807

Amatulli, G., McInerney, D., Sethi, T., Strobl, P., & Domisch, S. (2020). Geomorpho90m, empirical evaluation and accuracy assessment of global high-resolution geomorphometric layers. *Scientific Data*, *7*(1), Article 1. https://doi.org/10.1038/s41597-020-0479-6

Arndt, K. A., Oechel, W. C., Goodrich, J. P., Bailey, B. A., Kalhori, A., Hashemi, J., Sweeney, C., & Zona, D. (2019). Sensitivity of Methane Emissions to Later Soil Freezing in Arctic Tundra Ecosystems. *Journal of Geophysical Research: Biogeosciences*, *124*(8), 2595–2609. https://doi.org/10.1029/2019JG005242

Aydin, M., Verhulst, K. R., Saltzman, E. S., Battle, M. O., Montzka, S. A., Blake, D. R., Tang, Q., & Prather, M. J. (2011). Recent decreases in fossil-fuel emissions of ethane and methane derived from firn air. *Nature*, *476*(7359), Article 7359. https://doi.org/10.1038/nature10352

Baldocchi, D. D. (2003). Assessing the eddy covariance technique for evaluating carbon dioxide exchange rates of ecosystems: Past, present and future. *Global Change Biology*, *9*(4), 479–492. https://doi.org/10.1046/j.1365-2486.2003.00629.x

Baldocchi, D. D. (2020). How eddy covariance flux measurements have contributed to our understanding of Global Change Biology. *Global Change Biology*, *26*(1), 242–260. https://doi.org/10.1111/gcb.14807

Bansal, S., Creed, I. F., Tangen, B. A., Bridgham, S. D., Desai, A. R., Krauss, K. W., Neubauer, S. C., Noe, G. B., Rosenberry, D. O., Trettin, C., Wickland, K. P., Allen, S. T., Arias-Ortiz, A., Armitage, A. R., Baldocchi, D., Banerjee, K., Bastviken, D., Berg, P., Bogard, M. J., … Zhu, X. (2023). Practical Guide to Measuring Wetland Carbon Pools and Fluxes. *Wetlands*, *43*(8), 105. https://doi.org/10.1007/s13157-023-01722-2

Bao, T., Xu, X., Jia, G., Billesbach, D. P., & Sullivan, R. C. (2021). Much stronger tundra methane emissions during autumn freeze than spring thaw. *Global Change Biology*, *27*(2), 376–387. https://doi.org/10.1111/gcb.15421

https://doi.org/10.5194/essd-2024-84
Preprint. Discussion started: 3 April 2024

Baray, S., Jacob, D. J., Maasakkers, J. D., Sheng, J.-X., Sulprizio, M. P., Jones, D. B. A., Bloom, A. A., & McLaren, R. (2021). Estimating 2010–2015 anthropogenic and natural methane emissions in Canada using ECCC surface and GOSAT satellite observations. *Atmospheric Chemistry and Physics*, *21*(23), 18101–18121. https://doi.org/10.5194/acp-21-18101-2021

Bartsch, A., Efimova, A., Widhalm, B., Muri, X., von Baeckmann, C., Bergstedt, H., Ermokhina, K., Hugelius, G., Heim, B., & Leibmann, M. (2023a). Circumarctic landcover diversity considering wetness gradients. *EGUsphere*, 1–98. https://doi.org/10.5194/egusphere-2023-2295

Bartsch, A., Efimova, A., Widhalm, B., Muri, X., von Baeckmann, C., Bergstedt, H., Ermokhina, K., Hugelius, G., Heim, B., & Leibmann, M. (2023b). *Circumpolar Landcover Units* (1.0) [dataset]. Zenodo. https://doi.org/10.5281/zenodo.8399018

Beaulieu, J. J., Waldo, S., Balz, D. A., Barnett, W., Hall, A., Platz, M. C., & White, K. M. (2020). Methane and Carbon Dioxide Emissions From Reservoirs: Controls and Upscaling. *Journal of Geophysical Research: Biogeosciences*, *125*(12), e2019JG005474. https://doi.org/10.1029/2019JG005474

Bergamaschi, P., Houweling, S., Segers, A., Krol, M., Frankenberg, C., Scheepmaker, R. A., Dlugokencky, E., Wofsy, S. C., Kort, E. A., Sweeney, C., Schuck, T., Brenninkmeijer, C., Chen, H., Beck, V., & Gerbig, C. (2013). Atmospheric CH4 in the first decade of the 21st century: Inverse modeling analysis using SCIAMACHY satellite retrievals and NOAA surface measurements. *Journal of Geophysical Research: Atmospheres*, *118*(13), 7350–7369. https://doi.org/10.1002/jgrd.50480

Bloom, A. A., Bowman, K. W., Lee, M., Turner, A. J., Schroeder, R., Worden, J. R., Weidner, R., McDonald, K. C., & Jacob, D. J. (2017). A global wetland methane emissions and uncertainty dataset for atmospheric chemical transport models (WetCHARTs version 1.0). *Geoscientific Model Development*, *10*(6), 2141–2156. https://doi.org/10.5194/gmd-10-2141-2017

Bloom, A. A., Palmer, P. I., Fraser, A., Reay, D. S., & Frankenberg, C. (2010). Large-Scale Controls of Methanogenesis Inferred from Methane and Gravity Spaceborne Data. *Science*, *327*(5963), 322–325. https://doi.org/10.1126/science.1175176

Bodesheim, P., Jung, M., Gans, F., Mahecha, M. D., & Reichstein, M. (2018). Upscaled diurnal cycles of land–atmosphere fluxes: A new global half-hourly data product. *Earth System Science Data*, *10*(3), 1327–1365. https://doi.org/10.5194/essd-10-1327-2018

Breiman, L. (2001). Random Forests. *Machine Learning*, *45*(1), 5–32. https://doi.org/10.1023/A:1010933404324

Bruhwiler, L., Dlugokencky, E., Masarie, K., Ishizawa, M., Andrews, A., Miller, J., Sweeney, C., Tans, P., & Worthy, D. (2014). CarbonTracker-CH_4: An assimilation system for estimating emissions of atmospheric methane. *Atmospheric Chemistry and Physics*, *14*(16), 8269–8293. https://doi.org/10.5194/acp-14-8269-2014

Burdun, I., Bechtold, M., Aurela, M., De Lannoy, G., Desai, A. R., Humphreys, E., Kareksela, S., Komisarenko, V., Liimatainen, M., Marttila, H., Minkkinen, K., Nilsson, M. B., Ojanen, P., Salko, S.-S., Tuittila, E.-S., Uuemaa, E., & Rautiainen, M. (2023). Hidden becomes clear: Optical remote sensing of vegetation reveals water table dynamics in northern

https://doi.org/10.5194/essd-2024-84
Preprint. Discussion started: 3 April 2024

peatlands. *Remote Sensing of Environment*, *296*, 113736. https://doi.org/10.1016/j.rse.2023.113736

Chadburn, S. E., Aalto, T., Aurela, M., Baldocchi, D., Biasi, C., Boike, J., Burke, E. J., Comyn-Platt, E., Dolman, A. J., Duran-Rojas, C., Fan, Y., Friborg, T., Gao, Y., Gedney, N., Göckede, M., Hayman, G. D., Holl, D., Hugelius, G., Kutzbach, L., … Westermann, S. (2020). Modeled Microbial Dynamics Explain the Apparent Temperature Sensitivity of Wetland Methane Emissions. *Global Biogeochemical Cycles*, *34*(11), e2020GB006678. https://doi.org/10.1029/2020GB006678

Chang, K.-Y., Riley, W. J., Knox, S. H., Jackson, R. B., McNicol, G., Poulter, B., Aurela, M., Baldocchi, D., Bansal, S., Bohrer, G., Campbell, D. I., Cescatti, A., Chu, H., Delwiche, K. B., Desai, A. R., Euskirchen, E., Friborg, T., Goeckede, M., Helbig, M., … Zona, D. (2021). Substantial hysteresis in emergent temperature sensitivity of global wetland CH4 emissions. *Nature Communications*, *12*(1), Article 1. https://doi.org/10.1038/s41467-021-22452-1

Chang, R. Y.-W., Miller, C. E., Dinardo, S. J., Karion, A., Sweeney, C., Daube, B. C., Henderson, J. M., Mountain, M. E., Eluszkiewicz, J., Miller, J. B., Bruhwiler, L. M. P., & Wofsy, S. C. (2014). Methane emissions from Alaska in 2012 from CARVE airborne observations. *Proceedings of the National Academy of Sciences*, *111*(47), 16694–16699. https://doi.org/10.1073/pnas.1412953111

Chen, Y., Huang, C., Ticehurst, C., Merrin, L., & Thew, P. (2013). An Evaluation of MODIS Daily and 8-day Composite Products for Floodplain and Wetland Inundation Mapping. *Wetlands*, *33*(5), 823–835. https://doi.org/10.1007/s13157-013-0439-4

Choe, H., Chi, J., & Thorne, J. H. (2021). Mapping Potential Plant Species Richness over Large Areas with Deep Learning, MODIS, and Species Distribution Models. *Remote Sensing*, *13*(13), Article 13. https://doi.org/10.3390/rs13132490

Chu, H., Luo, X., Ouyang, Z., Chan, W. S., Dengel, S., Biraud, S. C., Torn, M. S., Metzger, S., Kumar, J., Arain, M. A., Arkebauer, T. J., Baldocchi, D., Bernacchi, C., Billesbach, D., Black, T. A., Blanken, P. D., Bohrer, G., Bracho, R., Brown, S., … Zona, D. (2021). Representativeness of Eddy-Covariance flux footprints for areas surrounding AmeriFlux sites. *Agricultural and Forest Meteorology*, *301–302*, 108350. https://doi.org/10.1016/j.agrformet.2021.108350

Colliander, A., Reichle, R. H., Crow, W. T., Cosh, M. H., Chen, F., Chan, S., Das, N. N., Bindlish, R., Chaubell, J., Kim, S., Liu, Q., O'Neill, P. E., Dunbar, R. S., Dang, L. B., Kimball, J. S., Jackson, T. J., Al-Jassar, H. K., Asanuma, J., Bhattacharya, B. K., … Yueh, S. H. (2022). Validation of Soil Moisture Data Products From the NASA SMAP Mission. *IEEE Journal of Selected Topics in Applied Earth Observations and Remote Sensing*, *15*, 364–392. https://doi.org/10.1109/JSTARS.2021.3124743

Davidson, S. J., Santos, M. J., Sloan, V. L., Reuss-Schmidt, K., Phoenix, G. K., Oechel, W. C., & Zona, D. (2017). Upscaling CH4 Fluxes Using High-Resolution Imagery in Arctic Tundra Ecosystems. *Remote Sensing*, *9*(12), Article 12. https://doi.org/10.3390/rs9121227

Delwiche, K. B., Knox, S. H., Malhotra, A., Fluet-Chouinard, E., McNicol, G., Feron, S., Ouyang, Z., Papale, D., Trotta, C., Canfora, E., Cheah, Y.-W., Christianson, D., Alberto, M. C. R., Alekseychik, P., Aurela, M., Baldocchi, D., Bansal, S., Billesbach, D. P., Bohrer, G., …

https://doi.org/10.5194/essd-2024-84
Preprint. Discussion started: 3 April 2024

Jackson, R. B. (2021). FLUXNET-CH_4: A global, multi-ecosystem dataset and analysis of methane seasonality from freshwater wetlands. *Earth System Science Data*, *13*(7), 3607–3689. https://doi.org/10.5194/essd-13-3607-2021

Entekhabi, D., Njoku, E. G., O'Neill, P. E., Kellogg, K. H., Crow, W. T., Edelstein, W. N., Entin, J. K., Goodman, S. D., Jackson, T. J., Johnson, J., Kimball, J., Piepmeier, J. R., Koster, R. D., Martin, N., McDonald, K. C., Moghaddam, M., Moran, S., Reichle, R., Shi, J. C., … Van Zyl, J. (2010). The Soil Moisture Active Passive (SMAP) Mission. *Proceedings of the IEEE*, *98*(5), 704–716. https://doi.org/10.1109/JPROC.2010.2043918

Euskirchen, E. S., Edgar, C. W., Kane, E. S., Waldrop, M. P., Neumann, R. B., Manies, K. L., Douglas, T. A., Dieleman, C., Jones, M. C., & Turetsky, M. R. (2024). Persistent net release of carbon dioxide and methane from an Alaskan lowland boreal peatland complex. *Global Change Biology*, *30*(1), e17139. https://doi.org/10.1111/gcb.17139

Fang, B., Lakshmi, V., Cosh, M., Liu, P.-W., Bindlish, R., & Jackson, T. J. (2022). A global 1-km downscaled SMAP soil moisture product based on thermal inertia theory. *Vadose Zone Journal*, *21*(2), e20182. https://doi.org/10.1002/vzj2.20182

Feron, S., Malhotra, A., Bansal, S., Fluet-Chouinard, E., McNicol, G., Knox, S. H., Delwiche, K. B., Cordero, R. R., Ouyang, Z., Zhang, Z., Poulter, B., & Jackson, R. B. (2024). Recent increases in annual, seasonal, and extreme methane fluxes driven by changes in climate and vegetation in boreal and temperate wetland ecosystems. *Global Change Biology*, *30*(1), e17131. https://doi.org/10.1111/gcb.17131

Friedlingstein, P., Jones, M. W., O'Sullivan, M., Andrew, R. M., Bakker, D. C. E., Hauck, J., Le Quéré, C., Peters, G. P., Peters, W., Pongratz, J., Sitch, S., Canadell, J. G., Ciais, P., Jackson, R. B., Alin, S. R., Anthoni, P., Bates, N. R., Becker, M., Bellouin, N., … Zeng, J. (2022). Global Carbon Budget 2021. *Earth System Science Data*, *14*(4), 1917–2005. https://doi.org/10.5194/essd-14-1917-2022

Gelaro, R., McCarty, W., Suárez, M. J., Todling, R., Molod, A., Takacs, L., Randles, C. A., Darmenov, A., Bosilovich, M. G., Reichle, R., Wargan, K., Coy, L., Cullather, R., Draper, C., Akella, S., Buchard, V., Conaty, A., Silva, A. M. da, Gu, W., … Zhao, B. (2017). The Modern-Era Retrospective Analysis for Research and Applications, Version 2 (MERRA-2). *Journal of Climate*, *30*(14), 5419–5454. https://doi.org/10.1175/JCLI-D-16-0758.1

Heimann, M. (2011). Enigma of the recent methane budget. *Nature*, *476*(7359), Article 7359. https://doi.org/10.1038/476157a

Herrington, T. C., Fletcher, C. G., & Kropp, H. (2022). Validation of Pan-Arctic Soil Temperatures in Modern Reanalysis and Data Assimilation Systems. *The Cryosphere Discussions*, 1–33. https://doi.org/10.5194/tc-2022-5

Högström, E., Heim, B., Bartsch, A., Bergstedt, H., & Pointner, G. (2018). Evaluation of a MetOp ASCAT-Derived Surface Soil Moisture Product in Tundra Environments. *Journal of Geophysical Research: Earth Surface*, *123*(12), 3190–3205. https://doi.org/10.1029/2018JF004658

Houborg, R., Soegaard, H., & Boegh, E. (2007). Combining vegetation index and model inversion methods for the extraction of key vegetation biophysical parameters using Terra and Aqua MODIS reflectance data. *Remote Sensing of Environment*, *106*(1), 39–58. https://doi.org/10.1016/j.rse.2006.07.016

https://doi.org/10.5194/essd-2024-84
Preprint. Discussion started: 3 April 2024

Hugelius, G., Loisel, J., Chadburn, S., Jackson, R. B., Jones, M., MacDonald, G., Marushchak, M., Olefeldt, D., Packalen, M., Siewert, M. B., Treat, C., Turetsky, M., Voigt, C., & Yu, Z. (2020). Large stocks of peatland carbon and nitrogen are vulnerable to permafrost thaw. *Proceedings of the National Academy of Sciences*, *117*(34), 20438–20446. https://doi.org/10.1073/pnas.1916387117

IPCC AR6. (2023). *AR6 Synthesis Report: Climate Change 2023 — IPCC*. https://www.ipcc.ch/report/sixth-assessment-report-cycle/

Irvin, J., Zhou, S., McNicol, G., Lu, F., Liu, V., Fluet-Chouinard, E., Ouyang, Z., Knox, S. H., Lucas-Moffat, A., Trotta, C., Papale, D., Vitale, D., Mammarella, I., Alekseychik, P., Aurela, M., Avati, A., Baldocchi, D., Bansal, S., Bohrer, G., … Jackson, R. B. (2021). Gap-filling eddy covariance methane fluxes: Comparison of machine learning model predictions and uncertainties at FLUXNET-CH4 wetlands. *Agricultural and Forest Meteorology*, *308–309*, 108528. https://doi.org/10.1016/j.agrformet.2021.108528

Iwata, H., Harazono, Y., Ueyama, M., Sakabe, A., Nagano, H., Kosugi, Y., Takahashi, K., & Kim, Y. (2015). Methane exchange in a poorly-drained black spruce forest over permafrost observed using the eddy covariance technique. *Agricultural and Forest Meteorology*, *214–215*, 157–168. https://doi.org/10.1016/j.agrformet.2015.08.252

Jiao, M., Zhao, L., Wang, C., Hu, G., Li, Y., Zhao, J., Zou, D., Xing, Z., Qiao, Y., Liu, G., Du, E., Xiao, M., & Hou, Y. (2023). Spatiotemporal Variations of Soil Temperature at 10 and 50 cm Depths in Permafrost Regions along the Qinghai-Tibet Engineering Corridor. *Remote Sensing*, *15*(2), Article 2. https://doi.org/10.3390/rs15020455

Johnson, M. S., Matthews, E., Bastviken, D., Deemer, B., Du, J., & Genovese, V. (2021). Spatiotemporal Methane Emission From Global Reservoirs. *Journal of Geophysical Research: Biogeosciences*, *126*(8), e2021JG006305. https://doi.org/10.1029/2021JG006305

Johnson, M. S., Matthews, E., Du, J., Genovese, V., & Bastviken, D. (2022). Methane Emission From Global Lakes: New Spatiotemporal Data and Observation-Driven Modeling of Methane Dynamics Indicates Lower Emissions. *Journal of Geophysical Research: Biogeosciences*, *127*(7), e2022JG006793. https://doi.org/10.1029/2022JG006793

Jung, M., Reichstein, M., Margolis, H. A., Cescatti, A., Richardson, A. D., Arain, M. A., Arneth, A., Bernhofer, C., Bonal, D., Chen, J., Gianelle, D., Gobron, N., Kiely, G., Kutsch, W., Lasslop, G., Law, B. E., Lindroth, A., Merbold, L., Montagnani, L., … Williams, C. (2011). Global patterns of land-atmosphere fluxes of carbon dioxide, latent heat, and sensible heat derived from eddy covariance, satellite, and meteorological observations. *Journal of Geophysical Research: Biogeosciences*, *116*(G3). https://doi.org/10.1029/2010JG001566

Jung, M., Schwalm, C., Migliavacca, M., Walther, S., Camps-Valls, G., Koirala, S., Anthoni, P., Besnard, S., Bodesheim, P., Carvalhais, N., Chevallier, F., Gans, F., Goll, D. S., Haverd, V., Köhler, P., Ichii, K., Jain, A. K., Liu, J., Lombardozzi, D., … Reichstein, M. (2020). Scaling carbon fluxes from eddy covariance sites to globe: Synthesis and evaluation of the FLUXCOM approach. *Biogeosciences*, *17*(5), 1343–1365. https://doi.org/10.5194/bg-17-1343-2020

Kim, Y., Johnson, M. S., Knox, S. H., Black, T. A., Dalmagro, H. J., Kang, M., Kim, J., & Baldocchi, D. (2020). Gap-filling approaches for eddy covariance methane fluxes: A

https://doi.org/10.5194/essd-2024-84
Preprint. Discussion started: 3 April 2024

comparison of three machine learning algorithms and a traditional method with principal component analysis. *Global Change Biology*, *26*(3), 1499–1518. https://doi.org/10.1111/gcb.14845

Kirschke, S., Bousquet, P., Ciais, P., Saunois, M., Canadell, J. G., Dlugokencky, E. J., Bergamaschi, P., Bergmann, D., Blake, D. R., Bruhwiler, L., Cameron-Smith, P., Castaldi, S., Chevallier, F., Feng, L., Fraser, A., Heimann, M., Hodson, E. L., Houweling, S., Josse, B., … Zeng, G. (2013). Three decades of global methane sources and sinks. *Nature Geoscience*, *6*(10), Article 10. https://doi.org/10.1038/ngeo1955

Knox, S. H., Bansal, S., McNicol, G., Schafer, K., Sturtevant, C., Ueyama, M., Valach, A. C., Baldocchi, D., Delwiche, K., Desai, A. R., Euskirchen, E., Liu, J., Lohila, A., Malhotra, A., Melling, L., Riley, W., Runkle, B. R. K., Turner, J., Vargas, R., … Jackson, R. B. (2021). Identifying dominant environmental predictors of freshwater wetland methane fluxes across diurnal to seasonal time scales. *Global Change Biology*, *27*(15), 3582–3604. https://doi.org/10.1111/gcb.15661

Knox, S. H., Jackson, R. B., Poulter, B., McNicol, G., Fluet-Chouinard, E., Zhang, Z., Hugelius, G., Bousquet, P., Canadell, J. G., Saunois, M., Papale, D., Chu, H., Keenan, T. F., Baldocchi, D., Torn, M. S., Mammarella, I., Trotta, C., Aurela, M., Bohrer, G., … Zona, D. (2019). FLUXNET-CH4 Synthesis Activity: Objectives, Observations, and Future Directions. *Bulletin of the American Meteorological Society*, *100*(12), 2607–2632. https://doi.org/10.1175/BAMS-D-18-0268.1

Kuhn, M. A., Varner, R. K., Bastviken, D., Crill, P., MacIntyre, S., Turetsky, M., Walter Anthony, K., McGuire, A. D., & Olefeldt, D. (2021). BAWLD-CH_4: A comprehensive dataset of methane fluxes from boreal and arctic ecosystems. *Earth System Science Data*, *13*(11), 5151–5189. https://doi.org/10.5194/essd-13-5151-2021

Kuter, S. (2021). Completing the machine learning saga in fractional snow cover estimation from MODIS Terra reflectance data: Random forests versus support vector regression. *Remote Sensing of Environment*, *255*, 112294. https://doi.org/10.1016/j.rse.2021.112294

Kyzivat, E. D., Smith, L. C., Garcia-Tigreros, F., Huang, C., Wang, C., Langhorst, T., Fayne, J. V., Harlan, M. E., Ishitsuka, Y., Feng, D., Dolan, W., Pitcher, L. H., Wickland, K. P., Dornblaser, M. M., Striegl, R. G., Pavelsky, T. M., Butman, D. E., & Gleason, C. J. (2022). The Importance of Lake Emergent Aquatic Vegetation for Estimating Arctic-Boreal Methane Emissions. *Journal of Geophysical Research: Biogeosciences*, *127*(6), e2021JG006635. https://doi.org/10.1029/2021JG006635

Larmola, T., Tuittila, E.-S., Tiirola, M., Nykänen, H., Martikainen, P. J., Yrjälä, K., Tuomivirta, T., & Fritze, H. (2010). The role of Sphagnum mosses in the methane cycling of a boreal mire. *Ecology*, *91*(8), 2356–2365. https://doi.org/10.1890/09-1343.1

Lehner, B., & Döll, P. (2004). Development and validation of a global database of lakes, reservoirs and wetlands. *Journal of Hydrology*, *296*(1), 1–22. https://doi.org/10.1016/j.jhydrol.2004.03.028

Li, M., Wu, P., & Ma, Z. (2020). A comprehensive evaluation of soil moisture and soil temperature from third-generation atmospheric and land reanalysis data sets. *International Journal of Climatology*, *40*(13), 5744–5766. https://doi.org/10.1002/joc.6549

https://doi.org/10.5194/essd-2024-84
Preprint. Discussion started: 3 April 2024

Li, T., Raivonen, M., Alekseychik, P., Aurela, M., Lohila, A., Zheng, X., Zhang, Q., Wang, G., Mammarella, I., Rinne, J., Yu, L., Xie, B., Vesala, T., & Zhang, W. (2016). Importance of vegetation classes in modeling CH4 emissions from boreal and subarctic wetlands in Finland. *Science of The Total Environment*, *572*, 1111–1122. https://doi.org/10.1016/j.scitotenv.2016.08.020

Liebner, S., Zeyer, J., Wagner, D., Schubert, C., Pfeiffer, E.-M., & Knoblauch, C. (2011). Methane oxidation associated with submerged brown mosses reduces methane emissions from Siberian polygonal tundra. *Journal of Ecology*, *99*(4), 914–922. https://doi.org/10.1111/j.1365-2745.2011.01823.x

Liu, L., Xu, S., Tang, J., Guan, K., Griffis, T. J., Erickson, M. D., Frie, A. L., Jia, X., Kim, T., Miller, L. T., Peng, B., Wu, S., Yang, Y., Zhou, W., Kumar, V., & Jin, Z. (2022). KGML-ag: A modeling framework of knowledge-guided machine learning to simulate agroecosystems: a case study of estimating N_2O emission using data from mesocosm experiments. *Geoscientific Model Development*, *15*(7), 2839–2858. https://doi.org/10.5194/gmd-15-2839-2022

Ludwig, S. M., Natali, S. M., Schade, J. D., Powell, M., Fiske, G., Schiferl, L. D., & Commane, R. (2023). Scaling waterbody carbon dioxide and methane fluxes in the arctic using an integrated terrestrial-aquatic approach. *Environmental Research Letters*, *18*(6), 064019. https://doi.org/10.1088/1748-9326/acd467

Ma, H., Zeng, J., Zhang, X., Fu, P., Zheng, D., Wigneron, J.-P., Chen, N., & Niyogi, D. (2021). Evaluation of six satellite- and model-based surface soil temperature datasets using global ground-based observations. *Remote Sensing of Environment*, *264*, 112605. https://doi.org/10.1016/j.rse.2021.112605

Masson-Delmotte, V., Zhai, P., Pirani, A., Connors, S. L., Péan, C., Berger, S., Caud, N., Chen, Y., Goldfarb, L., & Gomis, M. I. (2021). Climate change 2021: The physical science basis. *Contribution of Working Group I to the Sixth Assessment Report of the Intergovernmental Panel on Climate Change*, *2*.

Mastepanov, M., Sigsgaard, C., Dlugokencky, E. J., Houweling, S., Ström, L., Tamstorf, M. P., & Christensen, T. R. (2008). Large tundra methane burst during onset of freezing. *Nature*, *456*(7222), Article 7222. https://doi.org/10.1038/nature07464

Mavrovic, A., Sonnentag, O., Lemmetyinen, J., Voigt, C., Aurela, M., & Roy, A. (2024). *Winter methane fluxes over boreal and Arctic environments*. ESS Open Archive. https://doi.org/10.22541/essoar.170542245.58670859/v1

McGuire, A. D., Anderson, L. G., Christensen, T. R., Dallimore, S., Guo, L., Hayes, D. J., Heimann, M., Lorenson, T. D., Macdonald, R. W., & Roulet, N. (2009). Sensitivity of the carbon cycle in the Arctic to climate change. *Ecological Monographs*, *79*(4), 523–555. https://doi.org/10.1890/08-2025.1

McNicol, G., Fluet-Chouinard, E., Ouyang, Z., Knox, S., Zhang, Z., Aalto, T., Bansal, S., Chang, K.-Y., Chen, M., Delwiche, K., Feron, S., Goeckede, M., Liu, J., Malhotra, A., Melton, J. R., Riley, W., Vargas, R., Yuan, K., Ying, Q., … Jackson, R. B. (2023). Upscaling Wetland Methane Emissions From the FLUXNET-CH4 Eddy Covariance Network (UpCH4 v1.0): Model Development, Network Assessment, and Budget Comparison. *AGU Advances*, *4*(5), e2023AV000956. https://doi.org/10.1029/2023AV000956

https://doi.org/10.5194/essd-2024-84
Preprint. Discussion started: 3 April 2024

Open Access Earth System Science Data Discussions

Melack, J. M., & Hess, L. L. (2023). Areal extent of vegetative cover: A challenge to regional upscaling of methane emissions. *Aquatic Botany*, *184*, 103592. https://doi.org/10.1016/j.aquabot.2022.103592

Melton, J. R., Wania, R., Hodson, E. L., Poulter, B., Ringeval, B., Spahni, R., Bohn, T., Avis, C. A., Beerling, D. J., Chen, G., Eliseev, A. V., Denisov, S. N., Hopcroft, P. O., Lettenmaier, D. P., Riley, W. J., Singarayer, J. S., Subin, Z. M., Tian, H., Zürcher, S., … Kaplan, J. O. (2013). Present state of global wetland extent and wetland methane modelling: Conclusions from a model inter-comparison project (WETCHIMP). *Biogeosciences*, *10*(2), 753–788. https://doi.org/10.5194/bg-10-753-2013

Miller, S. M., Miller, C. E., Commane, R., Chang, R. Y.-W., Dinardo, S. J., Henderson, J. M., Karion, A., Lindaas, J., Melton, J. R., Miller, J. B., Sweeney, C., Wofsy, S. C., & Michalak, A. M. (2016). A multiyear estimate of methane fluxes in Alaska from CARVE atmospheric observations. *Global Biogeochemical Cycles*, *30*(10), 1441–1453. https://doi.org/10.1002/2016GB005419

Miner, K. R., Turetsky, M. R., Malina, E., Bartsch, A., Tamminen, J., McGuire, A. D., Fix, A., Sweeney, C., Elder, C. D., & Miller, C. E. (2022). Permafrost carbon emissions in a changing Arctic. *Nature Reviews Earth & Environment*, *3*(1), Article 1. https://doi.org/10.1038/s43017-021-00230-3

Murray-Hudson, M., Wolski, P., Cassidy, L., Brown, M. T., Thito, K., Kashe, K., & Mosimanyana, E. (2015). Remote Sensing-derived hydroperiod as a predictor of floodplain vegetation composition. *Wetlands Ecology and Management*, *23*(4), 603–616. https://doi.org/10.1007/s11273-014-9340-z

Natali, S. M., Watts, J. D., Rogers, B. M., Potter, S., Ludwig, S. M., Selbmann, A.-K., Sullivan, P. F., Abbott, B. W., Arndt, K. A., Birch, L., Björkman, M. P., Bloom, A. A., Celis, G., Christensen, T. R., Christiansen, C. T., Commane, R., Cooper, E. J., Crill, P., Czimczik, C., … Zona, D. (2019). Large loss of CO2 in winter observed across the northern permafrost region. *Nature Climate Change*, *9*(11), Article 11. https://doi.org/10.1038/s41558-019-0592-8

Olefeldt, D., Euskirchen, E. S., Harden, J., Kane, E., McGuire, A. D., Waldrop, M. P., & Turetsky, M. R. (2017). A decade of boreal rich fen greenhouse gas fluxes in response to natural and experimental water table variability. *Global Change Biology*, *23*(6), 2428–2440. https://doi.org/10.1111/gcb.13612

Olefeldt, D., Hovemyr, M., Kuhn, M. A., Bastviken, D., Bohn, T. J., Connolly, J., Crill, P., Euskirchen, E. S., Finkelstein, S. A., Genet, H., Grosse, G., Harris, L. I., Heffernan, L., Helbig, M., Hugelius, G., Hutchins, R., Juutinen, S., Lara, M. J., Malhotra, A., … Watts, J. D. (2021). The Boreal–Arctic Wetland and Lake Dataset (BAWLD). *Earth System Science Data*, *13*(11), 5127–5149. https://doi.org/10.5194/essd-13-5127-2021

Olefeldt, D., Turetsky, M. R., Crill, P. M., & McGuire, A. D. (2013). Environmental and physical controls on northern terrestrial methane emissions across permafrost zones. *Global Change Biology*, *19*(2), 589–603. https://doi.org/10.1111/gcb.12071

Osterkamp, T. E., Viereck, L., Shur, Y., Jorgenson, M. T., Racine, C., Doyle, A., & Boone, R. D. (2000). Observations of Thermokarst and Its Impact on Boreal Forests in Alaska, U.S.A. *Arctic, Antarctic, and Alpine Research*, *32*(3), 303–315. https://doi.org/10.1080/15230430.2000.12003368

https://doi.org/10.5194/essd-2024-84
Preprint. Discussion started: 3 April 2024

Ouyang, Z., Jackson, R. B., McNicol, G., Fluet-Chouinard, E., Runkle, B. R. K., Papale, D., Knox, S. H., Cooley, S., Delwiche, K. B., Feron, S., Irvin, J. A., Malhotra, A., Muddasir, M., Sabbatini, S., Alberto, Ma. C. R., Cescatti, A., Chen, C.-L., Dong, J., Fong, B. N., … Zhang, Y. (2023). Paddy rice methane emissions across Monsoon Asia. *Remote Sensing of Environment*, *284*, 113335. https://doi.org/10.1016/j.rse.2022.113335

Pallandt, M. M. T. A., Kumar, J., Mauritz, M., Schuur, E. A. G., Virkkala, A.-M., Celis, G., Hoffman, F. M., & Göckede, M. (2022). Representativeness assessment of the pan-Arctic eddy covariance site network and optimized future enhancements. *Biogeosciences*, *19*(3), 559–583. https://doi.org/10.5194/bg-19-559-2022

Pedregosa, F., Varoquaux, G., Gramfort, A., Michel, V., Thirion, B., Grisel, O., Blondel, M., Prettenhofer, P., Weiss, R., & Dubourg, V. (2011). Scikit-learn: Machine learning in Python. *The Journal of Machine Learning Research*, *12*, 2825–2830.

Peltola, O., Vesala, T., Gao, Y., Räty, O., Alekseychik, P., Aurela, M., Chojnicki, B., Desai, A. R., Dolman, A. J., Euskirchen, E. S., Friborg, T., Göckede, M., Helbig, M., Humphreys, E., Jackson, R. B., Jocher, G., Joos, F., Klatt, J., Knox, S. H., … Aalto, T. (2019). Monthly gridded data product of northern wetland methane emissions based on upscaling eddy covariance observations. *Earth System Science Data*, *11*(3), 1263–1289. https://doi.org/10.5194/essd-11-1263-2019

Peng, J., Loew, A., Merlin, O., & Verhoest, N. E. C. (2017). A review of spatial downscaling of satellite remotely sensed soil moisture. *Reviews of Geophysics*, *55*(2), 341–366. https://doi.org/10.1002/2016RG000543

Peng, S., Lin, X., Thompson, R. L., Xi, Y., Liu, G., Hauglustaine, D., Lan, X., Poulter, B., Ramonet, M., Saunois, M., Yin, Y., Zhang, Z., Zheng, B., & Ciais, P. (2022). Wetland emission and atmospheric sink changes explain methane growth in 2020. *Nature*, *612*(7940), Article 7940. https://doi.org/10.1038/s41586-022-05447-w

Prigent, C., Jimenez, C., & Bousquet, P. (2020). Satellite-Derived Global Surface Water Extent and Dynamics Over the Last 25 Years (GIEMS-2). *Journal of Geophysical Research: Atmospheres*, *125*(3), e2019JD030711. https://doi.org/10.1029/2019JD030711

Rawlins, M. A., Steele, M., Holland, M. M., Adam, J. C., Cherry, J. E., Francis, J. A., Groisman, P. Y., Hinzman, L. D., Huntington, T. G., Kane, D. L., Kimball, J. S., Kwok, R., Lammers, R. B., Lee, C. M., Lettenmaier, D. P., McDonald, K. C., Podest, E., Pundsack, J. W., Rudels, B., … Zhang, T. (2010). Analysis of the Arctic System for Freshwater Cycle Intensification: Observations and Expectations. *Journal of Climate*, *23*(21), 5715–5737. https://doi.org/10.1175/2010JCLI3421.1

Reichle, R. H., Lannoy, G. J. M. D., Liu, Q., Koster, R. D., Kimball, J. S., Crow, W. T., Ardizzone, J. V., Chakraborty, P., Collins, D. W., Conaty, A. L., Girotto, M., Jones, L. A., Kolassa, J., Lievens, H., Lucchesi, R. A., & Smith, E. B. (2017). Global Assessment of the SMAP Level-4 Surface and Root-Zone Soil Moisture Product Using Assimilation Diagnostics. *Journal of Hydrometeorology*, *18*(12), 3217–3237. https://doi.org/10.1175/JHM-D-17-0130.1

Reichstein, M., Camps-Valls, G., Stevens, B., Jung, M., Denzler, J., Carvalhais, N., & Prabhat. (2019). Deep learning and process understanding for data-driven Earth system science. *Nature*, *566*(7743), Article 7743. https://doi.org/10.1038/s41586-019-0912-1

https://doi.org/10.5194/essd-2024-84
Preprint. Discussion started: 3 April 2024

Rocher-Ros, G., Stanley, E. H., Loken, L. C., Casson, N. J., Raymond, P. A., Liu, S., Amatulli, G., & Sponseller, R. A. (2023). Global methane emissions from rivers and streams. *Nature*, *621*(7979), Article 7979. https://doi.org/10.1038/s41586-023-06344-6

Rosentreter, J. A., Borges, A. V., Deemer, B. R., Holgerson, M. A., Liu, S., Song, C., Melack, J., Raymond, P. A., Duarte, C. M., Allen, G. H., Olefeldt, D., Poulter, B., Battin, T. I., & Eyre, B. D. (2021). Half of global methane emissions come from highly variable aquatic ecosystem sources. *Nature Geoscience*, *14*(4), Article 4. https://doi.org/10.1038/s41561-021-00715-2

Rößger, N., Sachs, T., Wille, C., Boike, J., & Kutzbach, L. (2022). Seasonal increase of methane emissions linked to warming in Siberian tundra. *Nature Climate Change*, 1–6. https://doi.org/10.1038/s41558-022-01512-4

Saikia, P., Baruah, R. D., Singh, S. K., & Chaudhuri, P. K. (2020). Artificial Neural Networks in the domain of reservoir characterization: A review from shallow to deep models. *Computers & Geosciences*, *135*, 104357. https://doi.org/10.1016/j.cageo.2019.104357

Saunois, M., Stavert, A. R., Poulter, B., Bousquet, P., Canadell, J. G., Jackson, R. B., Raymond, P. A., Dlugokencky, E. J., Houweling, S., Patra, P. K., Ciais, P., Arora, V. K., Bastviken, D., Bergamaschi, P., Blake, D. R., Brailsford, G., Bruhwiler, L., Carlson, K. M., Carrol, M., … Zhuang, Q. (2020). The Global Methane Budget 2000–2017. *Earth System Science Data*, *12*(3), 1561–1623. https://doi.org/10.5194/essd-12-1561-2020

Schaaf, C. B., Gao, F., Strahler, A. H., Lucht, W., Li, X., Tsang, T., Strugnell, N. C., Zhang, X., Jin, Y., Muller, J.-P., Lewis, P., Barnsley, M., Hobson, P., Disney, M., Roberts, G., Dunderdale, M., Doll, C., d'Entremont, R. P., Hu, B., … Roy, D. (2002). First operational BRDF, albedo nadir reflectance products from MODIS. *Remote Sensing of Environment*, *83*(1), 135–148. https://doi.org/10.1016/S0034-4257(02)00091-3

Schiferl, L. D., Watts, J. D., Larson, E. J. L., Arndt, K. A., Biraud, S. C., Euskirchen, E. S., Goodrich, J. P., Henderson, J. M., Kalhori, A., McKain, K., Mountain, M. E., Munger, J. W., Oechel, W. C., Sweeney, C., Yi, Y., Zona, D., & Commane, R. (2022). Using atmospheric observations to quantify annual biogenic carbon dioxide fluxes on the Alaska North Slope. *Biogeosciences*, *19*(24), 5953–5972. https://doi.org/10.5194/bg-19-5953-2022

Smith, S. L., O'Neill, H. B., Isaksen, K., Noetzli, J., & Romanovsky, V. E. (2022). The changing thermal state of permafrost. *Nature Reviews Earth & Environment*, *3*(1), Article 1. https://doi.org/10.1038/s43017-021-00240-1

Spahni, R., Wania, R., Neef, L., van Weele, M., Pison, I., Bousquet, P., Frankenberg, C., Foster, P. N., Joos, F., Prentice, I. C., & van Velthoven, P. (2011). Constraining global methane emissions and uptake by ecosystems. *Biogeosciences*, *8*(6), 1643–1665. https://doi.org/10.5194/bg-8-1643-2011

Tramontana, G., Jung, M., Schwalm, C. R., Ichii, K., Camps-Valls, G., Ráduly, B., Reichstein, M., Arain, M. A., Cescatti, A., Kiely, G., Merbold, L., Serrano-Ortiz, P., Sickert, S., Wolf, S., & Papale, D. (2016). Predicting carbon dioxide and energy fluxes across global FLUXNET sites with regression algorithms. *Biogeosciences*, *13*(14), 4291–4313. https://doi.org/10.5194/bg-13-4291-2016

https://doi.org/10.5194/essd-2024-84
Preprint. Discussion started: 3 April 2024

Open Access Earth System Science Data Discussions

Treat, C. C., Bloom, A. A., & Marushchak, M. E. (2018). Nongrowing season methane emissions–a significant component of annual emissions across northern ecosystems. *Global Change Biology*, *24*(8), 3331–3343. https://doi.org/10.1111/gcb.14137

Turner, J., Desai, A. R., Thom, J., & Wickland, K. P. (2021). Lagged Wetland CH4 Flux Response in a Historically Wet Year. *Journal of Geophysical Research: Biogeosciences*, *126*(11), e2021JG006458. https://doi.org/10.1029/2021JG006458

Ueyama, M., Iwata, H., Endo, R., & Harazono, Y. (2023). Methane and carbon dioxide emissions from the forest floor of a black spruce forest on permafrost in interior Alaska. *Polar Science*, *35*, 100921. https://doi.org/10.1016/j.polar.2022.100921

Ueyama, M., Knox, S. H., Delwiche, K. B., Bansal, S., Riley, W. J., Baldocchi, D., Hirano, T., McNicol, G., Schafer, K., Windham-Myers, L., Poulter, B., Jackson, R. B., Chang, K.-Y., Chen, J., Chu, H., Desai, A. R., Gogo, S., Iwata, H., Kang, M., … Sachs, T. (2023). Modeled production, oxidation, and transport processes of wetland methane emissions in temperate, boreal, and Arctic regions. *Global Change Biology*, *29*(8), 2313–2334. https://doi.org/10.1111/gcb.16594

Upton, S., Reichstein, M., Gans, F., Peters, W., Kraft, B., & Bastos, A. (2023). Constraining biospheric carbon dioxide fluxes by combined top-down and bottom-up approaches. *EGUsphere*, 1–31. https://doi.org/10.5194/egusphere-2023-805

van Hulzen, J. B., Segers, R., van Bodegom, P. M., & Leffelaar, P. A. (1999). Temperature effects on soil methane production: An explanation for observed variability. *Soil Biology and Biochemistry*, *31*(14), 1919–1929. https://doi.org/10.1016/S0038-0717(99)00109-1

Villarreal, S., & Vargas, R. (2021). Representativeness of FLUXNET Sites Across Latin America. *Journal of Geophysical Research: Biogeosciences*, *126*(3), e2020JG006090. https://doi.org/10.1029/2020JG006090

Virkkala, A.-M., Aalto, J., Rogers, B. M., Tagesson, T., Treat, C. C., Natali, S. M., Watts, J. D., Potter, S., Lehtonen, A., Mauritz, M., Schuur, E. A. G., Kochendorfer, J., Zona, D., Oechel, W., Kobayashi, H., Humphreys, E., Goeckede, M., Iwata, H., Lafleur, P. M., … Luoto, M. (2021). Statistical upscaling of ecosystem CO2 fluxes across the terrestrial tundra and boreal domain: Regional patterns and uncertainties. *Global Change Biology*, *27*(17), 4040–4059. https://doi.org/10.1111/gcb.15659

Virkkala, A.-M., Niittynen, P., Kemppinen, J., Marushchak, M. E., Voigt, C., Hensgens, G., Kerttula, J., Happonen, K., Tyystjärvi, V., Biasi, C., Hultman, J., Rinne, J., & Luoto, M. (2023). High-resolution spatial patterns and drivers of terrestrial ecosystem carbon dioxide, methane, and nitrous oxide fluxes in the tundra. *Biogeosciences Discussions*, 1–29. https://doi.org/10.5194/bg-2023-61

Voigt, C., Virkkala, A.-M., Hould Gosselin, G., Bennett, K. A., Black, T. A., Detto, M., Chevrier-Dion, C., Guggenberger, G., Hashmi, W., Kohl, L., Kou, D., Marquis, C., Marsh, P., Marushchak, M. E., Nesic, Z., Nykänen, H., Saarela, T., Sauheitl, L., Walker, B., … Sonnentag, O. (2023). Arctic soil methane sink increases with drier conditions and higher ecosystem respiration. *Nature Climate Change*, *13*(10), Article 10. https://doi.org/10.1038/s41558-023-01785-3

Walsh, J. E. (2014). Intensified warming of the Arctic: Causes and impacts on middle latitudes. *Global and Planetary Change*, *117*, 52–63. https://doi.org/10.1016/j.gloplacha.2014.03.003

https://doi.org/10.5194/essd-2024-84
Preprint. Discussion started: 3 April 2024

Wang, W., Rinke, A., Moore, J. C., Ji, D., Cui, X., Peng, S., Lawrence, D. M., McGuire, A. D., Burke, E. J., Chen, X., Decharme, B., Koven, C., MacDougall, A., Saito, K., Zhang, W., Alkama, R., Bohn, T. J., Ciais, P., Delire, C., … Sherstiukov, A. B. (2016). Evaluation of air–soil temperature relationships simulated by land surface models during winter across the permafrost region. *The Cryosphere*, *10*(4), 1721–1737. https://doi.org/10.5194/tc-10-1721-2016

Wang, Z., Schaaf, C. B., Sun, Q., Shuai, Y., & Román, M. O. (2018). Capturing rapid land surface dynamics with Collection V006 MODIS BRDF/NBAR/Albedo (MCD43) products. *Remote Sensing of Environment*, *207*, 50–64. https://doi.org/10.1016/j.rse.2018.02.001

Watts, J. D., Farina, M., Kimball, J. S., Schiferl, L. D., Liu, Z., Arndt, K. A., Zona, D., Ballantyne, A., Euskirchen, E. S., Parmentier, F.-J. W., Helbig, M., Sonnentag, O., Tagesson, T., Rinne, J., Ikawa, H., Ueyama, M., Kobayashi, H., Sachs, T., Nadeau, D. F., … Oechel, W. C. (2023). Carbon uptake in Eurasian boreal forests dominates the high-latitude net ecosystem carbon budget. *Global Change Biology*, *29*(7), 1870–1889. https://doi.org/10.1111/gcb.16553

Watts, J. D., Kimball, J. S., Parmentier, F. J. W., Sachs, T., Rinne, J., Zona, D., Oechel, W., Tagesson, T., Jackowicz-Korczyński, M., & Aurela, M. (2014). A satellite data driven biophysical modeling approach for estimating northern peatland and tundra CO₂ and CH₄ fluxes. *Biogeosciences*, *11*(7), 1961–1980. https://doi.org/10.5194/bg-11-1961-2014

Wik, M., Varner, R. K., Anthony, K. W., MacIntyre, S., & Bastviken, D. (2016). Climate-sensitive northern lakes and ponds are critical components of methane release. *Nature Geoscience*, *9*(2), Article 2. https://doi.org/10.1038/ngeo2578

Wrona, E., Rowlandson, T. L., Nambiar, M., Berg, A. A., Colliander, A., & Marsh, P. (2017). Validation of the Soil Moisture Active Passive (SMAP) satellite soil moisture retrieval in an Arctic tundra environment. *Geophysical Research Letters*, *44*(9), 4152–4158. https://doi.org/10.1002/2017GL072946

Yamazaki, D., Ikeshima, D., Tawatari, R., Yamaguchi, T., O'Loughlin, F., Neal, J. C., Sampson, C. C., Kanae, S., & Bates, P. D. (2017). A high-accuracy map of global terrain elevations. *Geophysical Research Letters*, *44*(11), 5844–5853. https://doi.org/10.1002/2017GL072874

Ying, Q., Poulter, B., Watts, J. D., Arndt, K. A., Virkkala, A.-M., Bruhwiler, L., Oh, Y., Rogers, B. M., Natali, S. M., Sullivan, H., Schiferl, L. D., Elder, C., Peltola, O., Bartsch, A., Armstrong, A., Desai, A. R., Euskirchen, E., Göckede, M., Lehner, B., … Zhang, Z. (2024). *WetCH$_4$: A Machine Learning-based Upscaling of Methane Fluxes of Northern Wetlands during 2016-2022* [dataset]. Zenodo. https://doi.org/10.5281/zenodo.10802154

Yuan, K., Li, F., McNicol, G., Chen, M., Hoyt, A., Knox, S., Riley, W. J., Jackson, R., & Zhu, Q. (2024). Boreal–Arctic wetland methane emissions modulated by warming and vegetation activity. *Nature Climate Change*, 1–7. https://doi.org/10.1038/s41558-024-01933-3

Yuan, K., Zhu, Q., Li, F., Riley, W. J., Torn, M., Chu, H., McNicol, G., Chen, M., Knox, S., Delwiche, K., Wu, H., Baldocchi, D., Ma, H., Desai, A. R., Chen, J., Sachs, T., Ueyama, M., Sonnentag, O., Helbig, M., … Jackson, R. (2022). Causality guided machine learning model on wetland CH4 emissions across global wetlands. *Agricultural and Forest Meteorology*, *324*, 109115. https://doi.org/10.1016/j.agrformet.2022.109115

https://doi.org/10.5194/essd-2024-84
Preprint. Discussion started: 3 April 2024

Zhang, C., Comas, X., & Brodylo, D. (2020). A Remote Sensing Technique to Upscale Methane Emission Flux in a Subtropical Peatland. *Journal of Geophysical Research: Biogeosciences*, *125*(10), e2020JG006002. https://doi.org/10.1029/2020JG006002

Zhang, Z., Bansal, S., Chang, K.-Y., Fluet-Chouinard, E., Delwiche, K., Goeckede, M., Gustafson, A., Knox, S., Leppänen, A., Liu, L., Liu, J., Malhotra, A., Markkanen, T., McNicol, G., Melton, J. R., Miller, P. A., Peng, C., Raivonen, M., Riley, W. J., … Poulter, B. (2023). Characterizing Performance of Freshwater Wetland Methane Models Across Time Scales at FLUXNET-CH4 Sites Using Wavelet Analyses. *Journal of Geophysical Research: Biogeosciences*, *128*(11), e2022JG007259. https://doi.org/10.1029/2022JG007259

Zhang, Z., Fluet-Chouinard, E., Jensen, K., McDonald, K., Hugelius, G., Gumbricht, T., Carroll, M., Prigent, C., Bartsch, A., & Poulter, B. (2021). Development of the global dataset of Wetland Area and Dynamics for Methane Modeling (WAD2M). *Earth System Science Data*, *13*(5), 2001–2023. https://doi.org/10.5194/essd-13-2001-2021

Zhang, Z., Poulter, B., Feldman, A. F., Ying, Q., Ciais, P., Peng, S., & Li, X. (2023). Recent intensification of wetland methane feedback. *Nature Climate Change*, *13*(5), Article 5. https://doi.org/10.1038/s41558-023-01629-0

Zona, D., Gioli, B., Commane, R., Lindaas, J., Wofsy, S. C., Miller, C. E., Dinardo, S. J., Dengel, S., Sweeney, C., Karion, A., Chang, R. Y.-W., Henderson, J. M., Murphy, P. C., Goodrich, J. P., Moreaux, V., Liljedahl, A., Watts, J. D., Kimball, J. S., Lipson, D. A., & Oechel, W. C. (2016). Cold season emissions dominate the Arctic tundra methane budget. *Proceedings of the National Academy of Sciences*, *113*(1), 40–45. https://doi.org/10.1073/pnas.1516017113